ALMA MATER STUDIORUM · UNIVERSITÀ DI BOLOGNA

Scuola di Scienze
Dipartimento di Fisica e Astronomia
Corso di Laurea Magistrale in Fisica

Feasibility study of the MUonE experiment: reconstruction of the muon mean energy using the tracking system.

Relatore:
Prof. Domenico Galli

Correlatore:
Dott. Umberto Marconi

Presentata da:
Mattia Agozzino

Anno Accademico 2018/2019

A mio padre,
che una volta mi spiegò
perchè i piccioni non vengono folgorati
quando si appoggiano sui cavi dell'alta tensione.

Sommario

Il Modello Standard ha ricevuto molte conferme sperimentali negli ultimi decenni. Tuttavia sappiamo che esistono alcune lacune nella fisica delle particelle fondamentali che dovranno essere colmate. Una di queste è rappresentata dal momento magnetico anomalo del muone $a_\mu = (g-2)/2$. Questa quantità, come noto, presenta una differenza significativa di circa 3.5 σ tra il valore teorico e la misura sperimentale:
$\Delta a_\mu = a_\mu^{exp} - a_\mu^{SM} = 288(63)(49) \times 10^{-11}$. [1]

La precisione teorica nel calcolo di a_μ è limitata dalla conoscenza dei contributi adronici (QCD a bassa energia), in particolare il valore del contributo al primo ordine di vacuum-polarization a_μ^{HLO}. L'attuale determinazione di a_μ^{HLO} si basa sui risultati degli esperimenti agli acceleratori con eventi di annichilazione adronica a partire da collisioni e^+e^-.

L'obiettivo dell'esperimento MUonE è di ottenere una misura indipendente di a_μ^{HLO} e quindi arrivare a una più precisa determinazione teorica del momento magnetico anomalo del muone. Ci si propone di misurare a_μ^{HLO} utilizzando collisioni elastiche $\mu + e \to \mu + e$ per valutare il contributo adronico all'accoppiamento elettromagnetico $\Delta\alpha_{had}$ in regione di quadrimpulso trasferito di tipo space-like ($q^2 \leq 0$). Si propone di utilizzare i muoni del fascio M2 del CERN di 150 GeV su bersagli di berillio e di rivelare gli eventi elastici tracciando i prodotti dell'interazione. Il fascio M2 del CERN ha una dispersione in energia del 3.75%, che equivale a considerare muoni in ingresso con un energia di 150.0 ± 5.6 GeV. [14]

Per poter misurare $\Delta\alpha_{had}(q^2)$ occorre, in particolare, disporre di una conoscenza precisa della energia media dei muoni in ingresso dell'ordine di qualche MeV.

La struttura del rivelatore dell'esperimento MUonE è caratterizzata dall'impiego di molti moduli identici, disposti uno di seguito all'altro, ciascuno provvisto di bersaglio e sistema di tracciamento. Questo fa si che il solo sistema di rivelazione possibile per la misura dell'energia del muone sia il sistema di tracciamento.

Per misurare l'energia iniziale del muone proponiamo l'utilizzo del metodo template. Consideriamo la condizione di angoli di scattering uguali, e quindi che sia valida la relazione $\theta_\mu \simeq \theta_e$. In concreto richiediamo che gli angoli di uscita delle particelle dopo l'urto elastico siano compresi in un intervallo tra 2 e 3 mrad. Dato che in questo intervallo angolare le due particelle sono indistinguibili sulla sola base del sistema di tracciamento,

utilizziamo come osservabile l'angolo medio $\theta_s = (\theta_e + \theta_\mu)/2$. Simulando un insieme di eventi di energia iniziale assegnata secondo le specifiche del fascio M2, è possibile ottenere una distribuzione di θ_s. Questa è considerata come "pseudomisura" o misura di riferimento, ovvero come misura effettiva che potrebbe produrre il rivelatore dell'esperimento MUonE, della cui energia vogliamo determinare il valore.

La distribuzione di θ_s è ottenuta anche per altri valori di energia del fascio di muoni. Ciascun campione di eventi simulati produce una distibuzione di θ_s. Queste distribuzioni sono confrontate con quella di riferimento mediante un test di χ^2. Si ottiene così un insieme di valori di χ^2 in funzione dell'energia iniziale del fascio per ogni simulazione. Eseguendo un fit della funzione $\chi^2(E_\mu)$, si determina il valore del minimo che possiamo considerare come il valore più probabile per l'energia media del fascio di muoni della simulazione di riferimento.

Per ottenere i campioni di eventi simulati l'esperimento è stato descritto in un modello: le caratteristiche cinematiche dell'evento sono determinate secondo la sezione d'urto elastica; le interazioni con il bersaglio e con il materiale rivelatore sono state simulate considerando gli effetti di collisione elastica coulombiana multipla (multiple scattering). È stato possibile ottenere una stima dell'energia iniziale con incertezza inferiore a 10 MeV, utilizzando campioni di 10^7 eventi per ogni simulazione. È possibile ottenere campioni di questa taglia in condizioni reali in qualche ora di presa dati.

Abstract

The Standard Model obtained many experimental confirmations in the last years. However, we know there are still questions in particle physics that has to be answered. Among them it is the value of the muon anomalous magnetic moment $a_\mu = (g-2)/2$. This quantity presents nowadays a discrepancy between the theoretical value and the experimental measurement corresponding to a significativity of 3.5 σ: $\Delta a_\mu = a_\mu^{exp} - a_\mu^{SM} = 288(63)(49) \times 10^{-11}$. [1]

The theoretical prediction of a_{mu} is limited by the hadronic processes (low energy QCD), mainly by the leading order contribution a_μ^{HLO} due to the vacuum polarization. The present knowledge of a_μ^{HLO} relies on the results of the experiments at the accelerators with hadronic annihilations of e^+e^-.

Aim of MUonE is to reduce the uncertainty on the hadronic contribution a_μ^{HLO} to get a more precise measure of the muon anomalous magnetic moment. MUonE proposes to measure a_μ^{HLO} by using the elastic scattering $\mu(150\text{ GeV}) + e(\text{rest}) \to \mu + e$ to get the hadronic contribution to the electromagnetic coupling $\Delta\alpha_{had}$ for space-like transferred momenta. The MUonE proposal foresees the usage of the CERN M2 high intensity muon beam and low-Z Beryllium targets. The CERN M2 beam energy has a width of 3.75%, that implies the incoming muon energy has a value of 150.0 ± 5.6 GeV. [14]

In order to measure $\Delta\alpha_{had}(q^2)$ it is necessary to know very precisely the value of the incoming muon mean energy: it is necessary a knowledge of the initial energy with an uncertainty of about few MeV.

The MUonE detector is made of many identical stations (~ 40) located one downstream the others, each provided with a tin target and a tracking system. The tracking system is the only mean to measure the impinging muon mean energy. We propose on this purpose to use the template method.

We select elastic events with equal outcoming particles angles $\theta_\mu \simeq \theta_e$. In this condition the two particles are not distinguishable relying only on the angular information provided by the tracking system. For this reason, to determine the muon mean energy, we use the observable $\theta_s = (\theta_e + \theta_\mu)/2$. In practice for a muon beam energy of about 150 GeV the expected equal angles condition corresponds to 2.5 mrad. The interesting events are selected in the angular interval between 2 and 3 mrad.

To get a distribution of θ_s we generated a data set of events produced with muon mean

energy extrated according to the M2 beam specifications. This is a pseudo-measurement considered as the "real measure", that is the distribution we would obtain performing the MUonE experiment.

The distribution of θ_s is obtained for other varying the value of the initial muon mean energy in a neighbourhood of the nominal energy. These distributions are compared to the reference one with a χ^2 test. We get a set of χ^2 values, each for every energy consedered. Performing a fit of the χ^2 data set we determine the minimum value to be considered the most probable value for the muon mean energy reference value.

To obtain the distribution of θ_s we simulated the effect of the apparatus: the kinematic features of the event are determined according to the elastic scattering cross section; the interactions with the target and with the detector material are simulated using the Moliere multiple scattering model. We dimostrated that, using a set of 10^7 events, it will be possible to measure the muon beam mean energy with an uncertainty lower than 10 MeV. In the real experiment it will be possible to record such a statistics in few hours of data taking.

Contents

Chapter 1

The muon anomalous magnetic moment

1.1 Magnetic moment

In classical physics, the mechanical interaction between a magnetic field and an electrically charged particle is determined by the magnetic moment. Concerning a charge e orbiting around an axis in a magnetic field $\vec{B}$, the magnetic (orbital) moment is defined as:

$$\mu = i \cdot A = \frac{ev}{2\pi r}\,\pi r^2 = \frac{e \cdot mvr}{2m}, \tag{1.1}$$

where i is the current intensity due to the charge motion, A is the area swept out by the charge in its motion, v is the tangent velocity of the charge, r is the orbit radius and m is the particle mass. In vector notation:

$$\vec{\mu} = g_l\,\frac{e}{2m}\,\vec{L}, \qquad g_l = 1, \tag{1.2}$$

where the parameter g_l, i.e. the ratio between the magnetic moment $\vec{\mu}$ and the angular momentum $\vec{L}$, both properly normalized, is named *gyromagnetic ratio* or *g-factor*. In this case $g_l = 1$. The mechanical action of the magnetic field on the charge generates the torque:

$$\vec{M} = \vec{\mu} \times \vec{B}. \tag{1.3}$$

These considerations hold for any angular momentum, even for the *spin*, that quantum mechanics intrinsically assigns to each particle. In non-relativistic quantum mechanics, as well as in the Hamiltonian formalism, the orbital angular momentum is an operator with a complete set of eigenvectors for an electron that moves for example in a central field like the nucleus one [2]:

$$\begin{cases} \hat{H}u = E_n u \\ \hat{L}^2 u = \hbar^2 l\,(l+1)\,u \\ \hat{L}_z u = m_z \hbar u \end{cases} \tag{1.4}$$

The number of the possible values of the magnetic quantum number m_z is $2l+1$. It is usual to introduce the Bohr's magneton $\mu_B = \frac{e\,\hbar}{2m}$: for a generic angular momentum $\vec{J}$ we may write:

$$\vec{\mu} = g_j\,\frac{\mu_B}{\hbar}\,\vec{J}. \tag{1.5}$$

The first evidence of the spin dates back to the experiment of Stern and Gerlach (1922), performed using electrons. The discovery of the fourth degree of freedom of an electron is however attributed to Uhlenbeck and Goudsmit (1932): according to the Pauli exclusion principle, the spin allowed to explain, in a natural way, the atomic spectra under study. In paticular the Zeeman effect, caused by the interaction between the external magnetic field and the angular momentum $\vec{L}$ (orbital) and $\vec{S}$ (intrinsic), that is the spin-orbit coupling.

For a particle with spin, the magnetic moment is an intrinsic property and is obtained by replacing the angular momentum operator $\vec{L}$ with the spin $\vec{S}$:

$$\vec{S} = \frac{\sigma}{2}, \tag{1.6}$$

where σ_i (with $i = 1, 2, 3$) are Pauli matrices. The extension of the $\vec{L}$ operator properties to the spin $\vec{S}$ gives:

$$\begin{cases} \hat{S}^2 u = \hbar^2 s\,(s+1)\,u \\ \hat{S}_z u = m_s \hbar u \end{cases} \tag{1.7}$$

together with the definition of the intrinsic magnetic moment:

$$\vec{\mu} = g_s\,\frac{\mu_B}{\hbar}\,\vec{S} \tag{1.8}$$

The observations show that the possible values of the spin are only two, which implies $s = \frac{1}{2}$, according to he relation $2s+1 = 2$. Moreover unlike the agular contribution (where $g_l = 1$), in the spin case must be:

$$g_s = 2, \tag{1.9}$$

in order to be in accord with the experimental observation. The theoretical explanation of the empirical fact is included in the Dirac's theory. In the non-relativistic limit, the Dirac equation for an electron interacting in the electromagnetic field

$$A^\mu = (\phi, \vec{A}), \tag{1.10}$$

gives the Pauli equation:

$$\mathrm{i}\,\hbar\,\frac{\partial}{\partial t}\,|\psi\rangle = \left[\frac{\left(\vec{p} - e\vec{A}\right)^2}{2m_e} - \frac{e}{m_e}\,\vec{S}\cdot\vec{B} + e\,\phi\right]|\psi\rangle \tag{1.11}$$

where, in the square brackets, the first term represents the kinetic term, the second is the coupling between the spin and the magnetic field, and the last one is the coupling between the electric potential and the charge. Comparing the second contribution with Eq. (1.8), the theory predicts for the spin g-factor $g_s = 2$, as well as for all the point-like particles of spin $s = \frac{1}{2}$. As intrinsic property of matter, the spin arises naturally from Dirac's field equation and is one of its most remarkable achievement.

1.2 Schwinger calculus

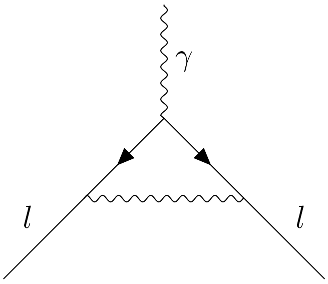

Figure 1.1: Lowest order QED contribution to the muon anomalous magnetic moment.

Fig. (1.1) shows the first order contribution to the magnetic moment by the virtual vacuum polarization process of QED. In 1948 Schwinger calculated the impact of this diagram to the electron g-factor. Recalling the Eq. (1.8), it is possible to define the anomaly a_μ as the deviation from Dirac's prediction:

$$g_\mu = 2\,(1 + a_\mu) \quad \Rightarrow \quad a_\mu = \frac{g_\mu - 2}{2}. \tag{1.12}$$

Hence the expression "$g - 2$" becomes a synonym for anomalus magnetic moment. Schwinger's a famous QED calculation predicts at first order:

$$a_\mu = \frac{\alpha}{2\pi} \sim 0.001161 \quad \Rightarrow \quad g_\mu^{th} = 2\cdot 1.001161, \tag{1.13}$$

so:

$$\vec{\mu}_s = g\,\frac{\mu_B}{\hbar}\,\vec{S} = 2\left(1 + \frac{\alpha}{2\pi}\right)\frac{\mu_B}{\hbar}\,\vec{S}. \tag{1.14}$$

In the same year Kusch and Foley obtained experimentally:

$$g_\mu^{exp} = 2\,(1.00119 \pm 0.00005)\,. \tag{1.15}$$

This result agrees with the Schwinger's prediction ad it is one of the first QED triumphs. The confirmation of the perturbative method gave start to higher order calculation and fixed the standard framework within which the most of the future calculations about the radiative corrections would be obtained. From the ~ 5 significant figures of the Kusch and Foley measurement, we have moved on to the 9 of the BNL measure.

1.3 Standard Model prediction to the muon $g-2$

In the Standard Model, the anomaly a_μ can be expressed as the sum of three contributions:

$$a_\mu^{SM} = a_\mu^{QED} + a_\mu^{EW} + a_\mu^{had}. \tag{1.16}$$

A precise prediction of this quantity is possible as the theory is renormalizable. So the anomalous magnetic moment has become one of the best observables to test it. The electromagnetic and weak terms can be calculated with extreme precision by perturbative calculations. The hadronic one, instead, must rely on experimental data and so it presents the biggest uncertainty. The $g-2$ is a low energy observable and in this region it is not possible the perturbative QCD treatment, because of the confinement. The issue of the hadronic contribution will be addressed in the following paragraphs.

1.3.1 QED contributions

In QED, the anomaly a_μ becomes a perturbative expansion in a $\frac{\alpha}{\pi}$:

$$a_\mu = \sum_j C_j \left(\frac{\alpha}{\pi}\right)^j \tag{1.17}$$

To date, theoretical calculations have reached the fifth perturbative order. Below the successive contributions and the main authors of the relative calculations:

$$\begin{aligned}
a_\mu^{QED} &= \frac{1}{2}\frac{\alpha}{\pi} && \text{[Schwinger 1948]}\\
&+ 0.765857426(16)\left(\frac{\alpha}{\pi}\right)^2 && \text{[Sommerfield 1957]}\\
&+ 24.05050988(28)\left(\frac{\alpha}{\pi}\right)^3 && \text{[Remiddi, Laporta 1995, 1996]}\\
&+ 130.8796(63)\left(\frac{\alpha}{\pi}\right)^4 && \text{[Kinoshita 1981, 2012]}\\
&+ 753.29(1.04)\left(\frac{\alpha}{\pi}\right)^5 && \text{[Kinoshita 2014]}
\end{aligned} \tag{1.18}$$

If we sum these five contributions, which are dominated by the first order calculated by Schwinger (1.14), we get:

$$a_\mu^{QED} = 0.00116584718951(22)(77). \tag{1.19}$$

The first error arises from the coefficients of the perturbative development, the second from the fine structure constant α, measured with Rubidium nuclei, which provides a new determination of the constant independent from the electron magnetic anomaly a_e, from which α was traditionally extracted.

1.3.2 EW contributions

The electroweak contribution is the smallest one, as it is suppressed by the factor $(m_\mu/M_W)^2$, compared to the QED. This contribution involves the massive bosons $W^\pm$, Z^0 and the Higgs. One-loop calculation leads to [3]:

$$\begin{aligned} a_\mu^{EW}[1\text{ loop}] &= \frac{5G_\mu m_\mu^2}{24\sqrt{2}\pi^2} + \left[1 + \frac{1}{5}\left(1 - 4\sin^2\theta_W\right)^2 + \mathcal{O}\left(\frac{m_\mu^2}{M_{Z,W,H}^2}\right)\right] = \\ &= 19.48 \times 10^{-10}, \end{aligned} \tag{1.20}$$

where $\sin^2\theta_W = 1 - M_W^2/M_Z^2 \approx 0.233$ is the electroweak angle and $G_\mu \approx 1.166 \times 10^{-5}\text{GeV}^{-2}$ is the Fermi coupling constant. The contribution to two loops also contains an hadronic part and must be included as it is not negligible (and negative). Using the Higgs boson mass value $M_H = (125.6 \pm 1.5)\text{GeV}$, one can get:

$$a_\mu^{EW}[2\text{ loops}] = -4.12(0.10) \times 10^{-10}, \tag{1.21}$$

where the error esserially depends on the hadronic loop uncertainties. Adding up the two terms:

$$a_\mu^{EW} = 15.36(0.10) \times 10^{-10}. \tag{1.22}$$

1.3.3 Hadronic contribution

Strong interactions allow perturbative calculations only for energy scales higher than few GeV, where one enters the regime of asymptotic freedom. The hadronic bubble in Fig. (2.2) cannot be calculated with the same method used for the first two contributions, EM and EW. Anyway most of the hadronic effects are vacuum polarization corrections, divided into leading and next-to-leading order:

$$a_\mu^{had\ VP} = a_\mu^{HLO} + a_\mu^{HNLO}. \tag{1.23}$$

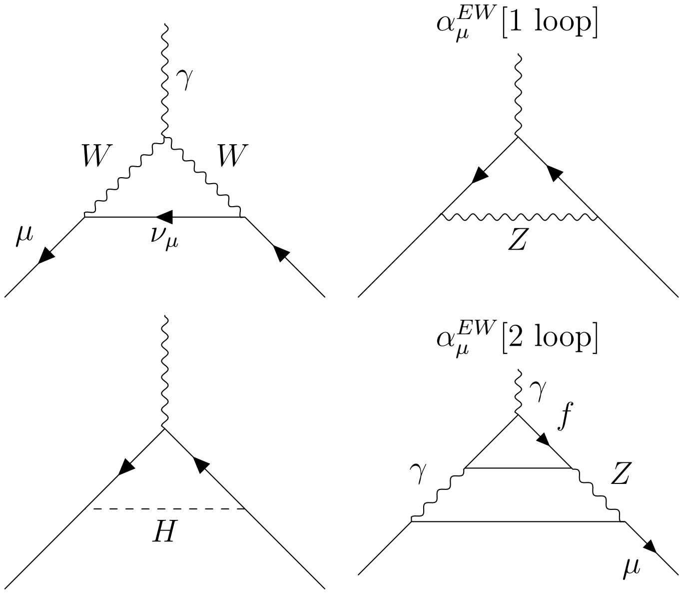

Figure 1.2: 1-loop and 2-loops electroweak contributions to the muon anomalous magnetic moment.

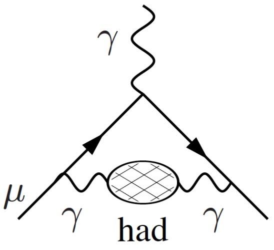

Figure 1.3: Hadronic vacuum polarization contribution at leading order to the muon anomalous magnetic moment.

The leading-order hadronic contribution to the muon $g-2$ is given by the formula [4]

$$a_\mu^{HLO} = \frac{\alpha}{\pi^2}\int_0^\infty \frac{ds}{s} K(s) \Im \prod_{had}(s+\epsilon), \tag{1.24}$$

where $\prod_{had}(s)$ is the hadronic part of the photon vacuum polarization, $\epsilon > 0$,

$$K(s) = \int_0^1 dx \frac{x^2(1-x)}{x^2 + (1-x)(s/m_\mu^2)} \tag{1.25}$$

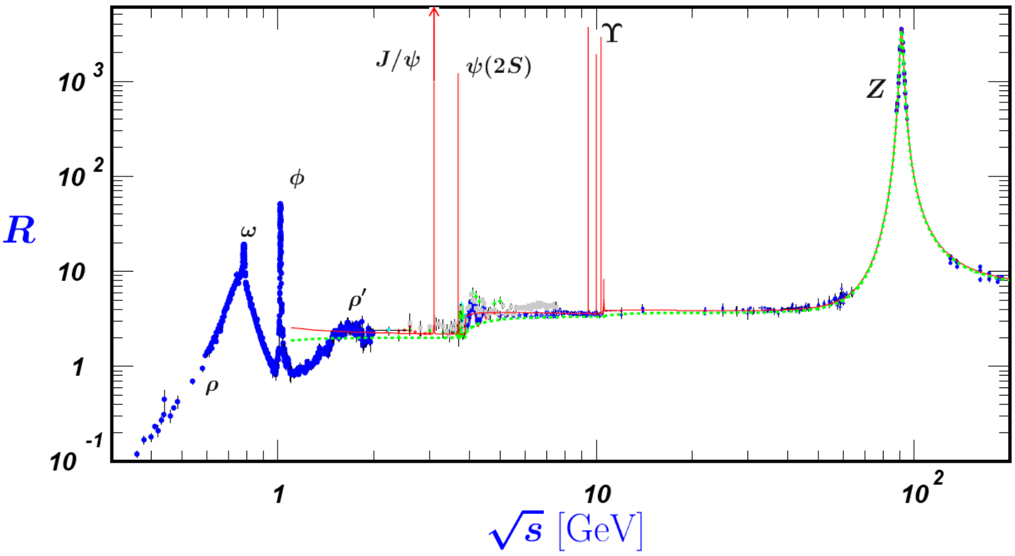

Figure 1.4: Hadronic cross section from PDG [3].

is a positive kernel function, and m_μ is the muon mass. As the total cross section for hadronic production in low-energy e^+e^- annihilations is related to the imaginary part of $\prod_{had}(s)$ via the optical theorem, the dispersion integral in Eq. (1.24) is computed intedrating experimental time-like $(s\ 0)$ data up to a certain value of s. The high-energy tail of integral is calculated using perturbative QCD. Using the R hadronic ratio, normalized to the cross section $e^+e^- \longrightarrow \mu^+\mu^-$ (Fig. (1.4)):

$$R(s) \equiv \frac{\sigma^{(0)}(e^+e^- \longrightarrow \gamma^* \longrightarrow \text{hadrons})}{4\pi\alpha^2/3s}, \tag{1.26}$$

which shows that the hadronic leading order contribution a_μ^{HLO} can be obtained from the following dispersion integral:

$$a_\mu^{HLO} = \left(\frac{\alpha m_\mu}{3\pi}\right)^2 \left(\int_{m_{\pi^0}^2}^{E_{cut}^2} \frac{R^{data}(s)\hat{K}(s)}{s^2} ds + \int_{E_{cut}^2}^{\infty} \frac{R^{pQCD}(s)\hat{K}(s)}{s^2} ds \right), \tag{1.27}$$

where E_{cut} is the energy up to which the data must be used and from where it is possible to use the perturbative QCD, the rescaled kernel function $\hat{K}(s) = 3s/m_\mu^2 K(s)$ is a smooth function rising from 0.39 for $s = m_{\pi^0}^2$ to 1 for $s \to \infty$. The $\rho(770)$ resonance represent the main contribution to a_μ^{HLO}.

Currently, the avaiable $\sigma(e^+e^- \longrightarrow \text{hadrons})$ data give a leading-order hadronic vacuum polarization contribution of [5]

$$a_\mu^{HLO} = 6\,923(42)(3) \times 10^{-11}, \tag{1.28}$$

where the first error is experimental (dominated by systematic uncertainties), and the second due to perturbative QCD, which is used at intermediate and large energies to predict the contribution from the quark-antiquark continuum.

Higher order, $\mathcal{O}(\alpha^3)$, hadronic contributions are obtained from dispersion relations using the same $e^+e^- \longrightarrow$ hadrons data [6], giving $a_\mu^{Disp,HNLO} = (-98.4 \pm 0.6) \times 10^{-11}$, along with model-dependent estimates of the hadronic light-by-light scattering contribution, $a_\mu^{LbL,HNLO}$. Following, one finds for the sum of the two terms [10]

$$a_\mu^{HNLO} = 7(26) \times 10^{-11}, \tag{1.29}$$

where the error is dominated by hadronic light-by-light uncertainties.

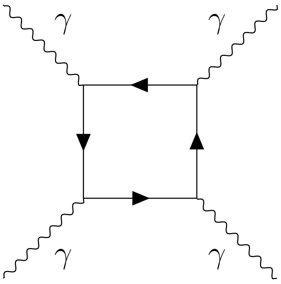

Figure 1.5: Light-by-light scattering diagram.

Adding Eqs. (1.19), (1.22), (1.28) and (1.29) gives the representative e^+e^- data based SM prediction [3]

$$a_\mu^{SM} = 116\,591\,803\,(1)(42)(26) \times 10^{-11}, \tag{1.30}$$

where the errors are due to the electroweak, lowest-order hadronic, and higher-order hadronic contributions, respectively.

The finest measure avaiable for a_μ^{exp} come from Brookhaven National Lab (BNL), where the E821 experiment studied the precession of μ^+ and μ^- in a constant external magnetic field as they circulated in a confining storage ring. It found [1]

$$\begin{aligned} a_{\mu+}^{exp} &= 11\,659\,204(6)(5) \times 10^{-10}, \\ a_{\mu-}^{exp} &= 11\,659\,215(8)(3) \times 10^{-10}, \end{aligned} \tag{1.31}$$

where the first error is statistical and the second systematic. Assuming CPT invariance and taking into account correlations between systematic uncertainties, one finds for their average [1]

$$a_\mu^{exp} = 11\,659\,209.1(5.4)(3.3) \times 10^{-10}. \tag{1.32}$$

The difference between experiment and theory

$$\Delta a_\mu = a_\mu^{exp} - a_\mu^{SM} = 288(63)(49) \times 10^{-11}, \tag{1.33}$$

(with all errors combined in quadrature) represents an interesting but not yet conclusive discrepancy of 3.6 times the estimated 1σ error.

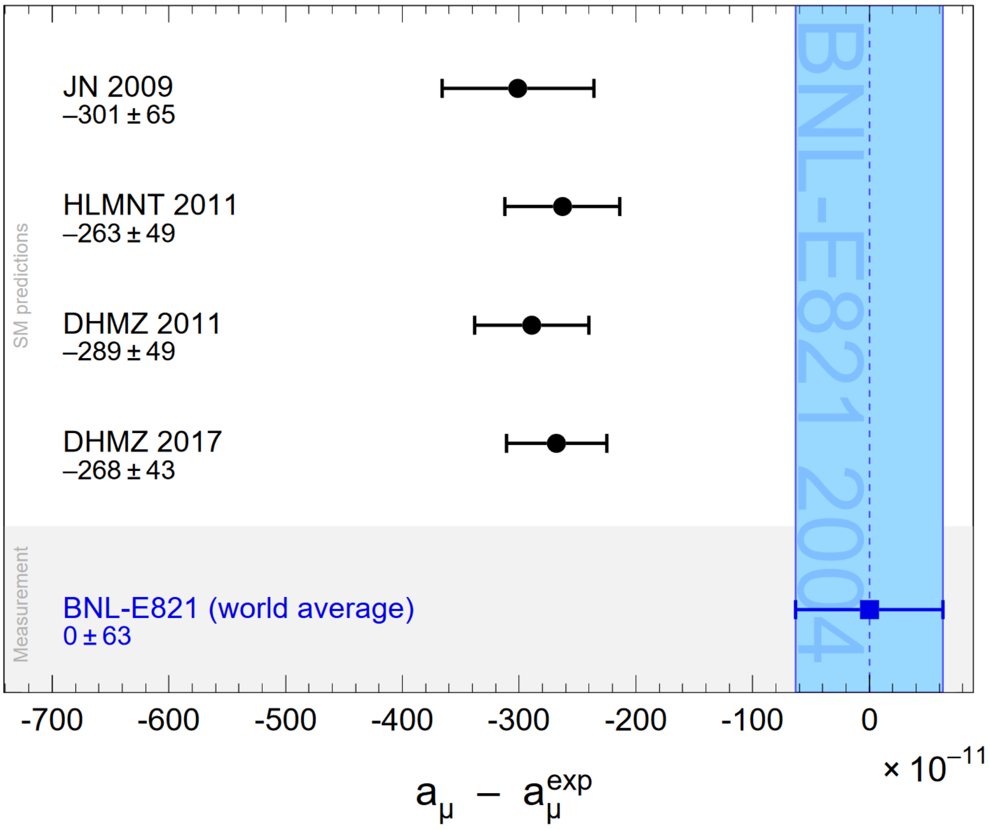

Figure 1.6: Compilation of recent published results for a_μ (in units of 10^{-11}), subtracted by the central by the central value of the experimental average (1.32). The shaded band indicates the size of the experimental uncertainty. The SM predictions are taken from: JN 2009 [7], HLMNT 2011 [8], DHMZ 2011 [5], DHMZ 2017 [9].

Chapter 2

The MUonE project

2.1 A new way to measure a_μ^{had} via space-like data

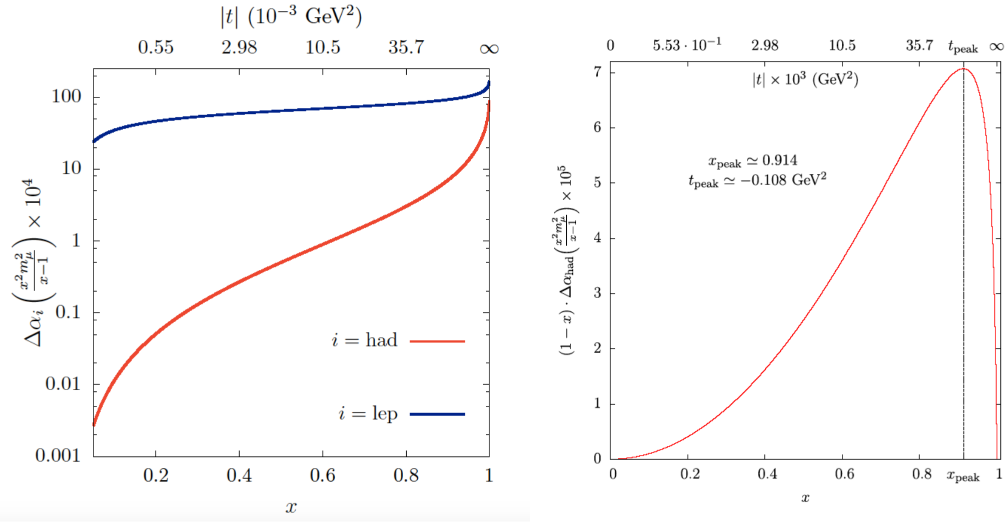

Figure 2.1: (left) Leptonic and hadronic contribution to the running of α. (right) The integrand in Eq. (2.9) from which can be determined a_μ^{HLO} [12].

The leading-order hadronic contribution (HLO) to the muon is calculable as showed above in Eq. (1.24), that is: [4]

$$a_\mu^{HLO} = \frac{\alpha}{\pi^2} \int_0^\infty \frac{ds}{s} K(s) \Im \prod_{had}(s), \tag{2.1}$$

where, as we said,

$$K(s) = \int_0^1 dx \frac{x^2(1-x)}{x^2 + (1-x)(s/m_\mu^2)}. \tag{2.2}$$

The integral defining a_μ^{HLO} is determined by the optical theorem [4], which links the e^+e^- hadronic production cross section to the imaginary part of $\prod_{had}(s)$, the hadronic contribution to the photon vacuum polarization.

The new method proposed by MUonE consists in changing the integration order between x and s, to get:

$$a_\mu^{HLO} = \frac{\alpha}{\pi^2}\int_0^1 dx m_\mu^2 x^2 \int_0^\infty \frac{ds}{s}\frac{\Im\prod_{had}(s)}{\frac{x^2 m_\mu^2}{1-x} + s}. \tag{2.3}$$

Using the dispertion relation:

$$\bar{\prod}_{had}[t(x)] \equiv \prod_{had}(t) - \prod_{had}(0) = \frac{t}{\pi}\int_0^\infty \frac{ds}{s}\frac{\Im\prod_{had}(s)}{s-t} \tag{2.4}$$

and defining the variable t as:

$$t(x) \equiv \frac{x^2 m_\mu^2}{x-1} < 0, \tag{2.5}$$

with $-\infty < t < 0$, Eq. (2.3) can be written as:

$$a_\mu^{HLO} = \frac{\alpha}{\pi^2}\int_0^1 dx(x-1)\bar{\prod_{had}}[t(x)]. \tag{2.6}$$

This relation indicates that t can be interpreted as the Mandelstam t variable. As $\Im\prod_{had}(t) = 0$ for negative t, Eq. (2.6) can be written in the form:

$$a_\mu^{HLO} = \frac{\alpha}{\pi}\int_0^1 dx(x-1)\Re\bar{\prod_{had}}[t(x)]. \tag{2.7}$$

$\Delta\alpha(t)$ is linked to the photon vacuum polarization by:

$$\Delta\alpha[t(x)] = -\Re\bar{\prod_{lep}}[t(x)] - \Re\bar{\prod_{had}}[t(x)]. \tag{2.8}$$

Therefore, considering $\Delta\alpha_{had}(t)$ we can rewrite Eq. (2.7) as [13]:

$$\boxed{a_\mu^{HLO} = \frac{\alpha}{\pi}\int_0^1 dx(1-x)\Delta\alpha_{had}[t(x)]}. \tag{2.9}$$

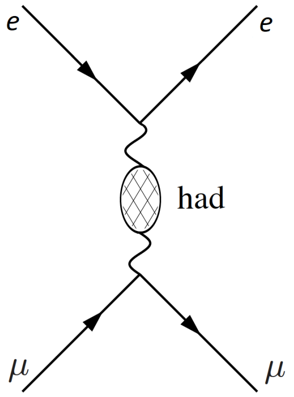

Figure 2.2: Hadronic contribution in the $\mu e \longrightarrow \mu e$ scattering event.

This is the fundamental feature of the MUonE proposal: it allows to calculate a_μ^{HLO} on the basis of $\Delta a_{had}(t)$, that is the hadronic contribution to the QED coupling running for space-like transferred momenta.

The rotation of the Feynman diagram (from s-channel annihilation to t-channel scattering) simplifies the calculation for the integral for a_μ^{HLO}. The space-like integrand function in Eq. (2.9), shown in Fig. 2.1, is smooth and free of resonances, differently to what happens in time-like approach. Thanks to this feature, it could be possible with a single scattering experiment to determine a_μ^{HLO}.

2.2 Experimental proposal

The MUonE proposal is to use the Eq. (2.9) to determine a_μ^{HLO} by measuring the running of α for space-like transferred momenta The proposed technique is similar to the one used for the measurement of the pion form factor. It is very appealing for the following reasons:

(i) It is a t-channel process, making the dependance on t of the differential cross section proportional to $|\alpha(t)/\alpha(0)|^2$:

$$\frac{d\sigma}{dt} = \frac{d\sigma_0}{dt}\left|\frac{\alpha(t)}{\alpha(0)}\right|^2 \tag{2.10}$$

where $d\sigma_0/dt$ is the effective Born cross section, including virtual and soft photons. The vacuum polarization effect, in the leading photon t-channel exchange, is incorporated in the running of α and gives rise to the factor $|\alpha(t)/\alpha(0)|^2$. It is understood that for a high precision measurement also higher-order radiative corrections must be included.

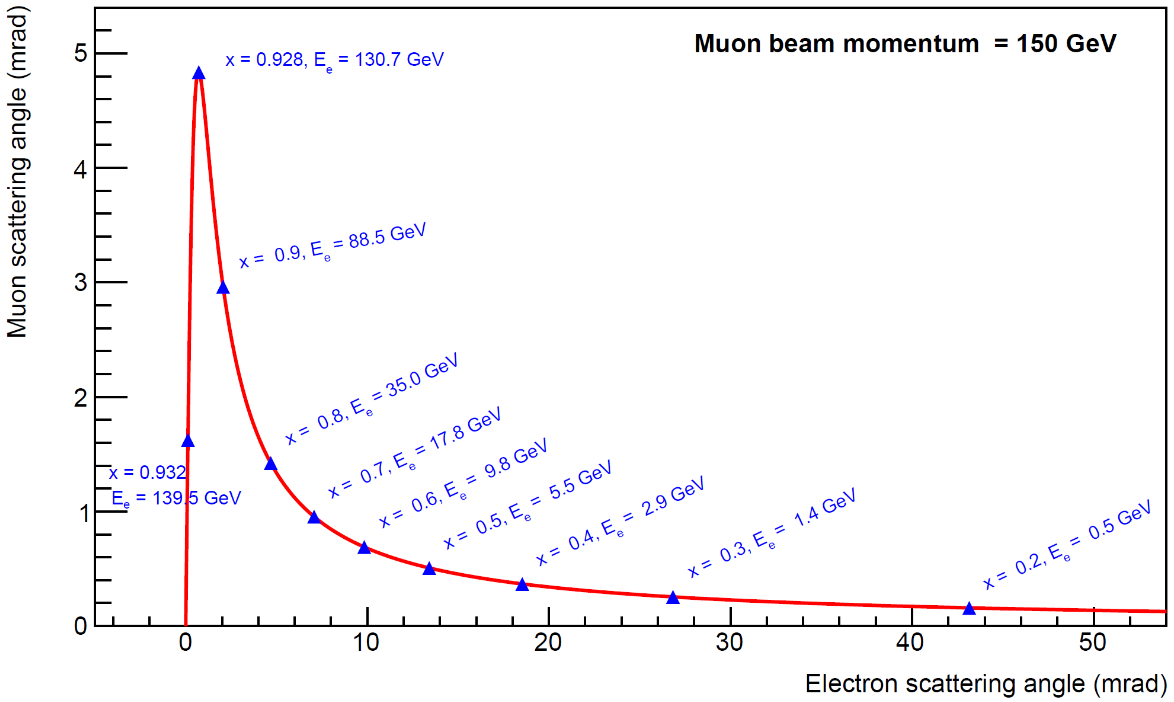

Figure 2.3: The relation between the muon and electron scattering angles for 150 GeV incident muon beam momentum. Blue triangles indicate reference values of the Feynman's x and electron energy.

(ii) Given the incoming muon energy E^i_μ, in a fixed-target experiment, the t variable is related to the energy of the scattered electron E^f_e and to its angle θ^f_e:

$$t = (p_\mu - p'_\mu)^2 = (p_e - p'_e)^2 = 2m_e^2 - 2m_e^2 E'_e, \tag{2.11}$$

$$s = (p_\mu - p'_e)^2 = (p_\mu - p'_e)^2 = m_\mu^2 + m_e^2 + 2m_e^2 E'_\mu, \tag{2.12}$$

$$E'_e = m_e \frac{1 + r^2 \cos^2\theta_e}{1 - r^2 \cos^2\theta_e}, \quad \theta'_e = \arccos\left(\frac{1}{r}\sqrt{\frac{E'_e - m_e}{E'_e + m_e}}\right), \tag{2.13}$$

where

$$r \equiv \frac{\sqrt{(E_\mu)^2 - m_\mu^2}}{E_\mu + m_e}. \tag{2.14}$$

The angle θ'_e spans the range (0-31.85) mrad for the electron energy E'_e in the range (1-139.8) GeV (the low-energy cut at 1 GeV is arbitrary).

(*iii*) For $E_\mu = 150$ GeV, it turns out that $s \simeq 0.164463$ GeV^2 and -0.142893 GeV$^2 < t < 0$ GeV^2. It implies that the region of x extends up to 0.93, while the peak of the integrand function of Eq. (2.9) is at $x_{peak} = 0.914$, corresponding to an electron scattering angle of 1.5 mrad, as visible in Fig. 2.1 (right).

(*iv*) The angles of the scattered electron and muon are corrrelated as shown in Fig. 2.3. This constraint is extremely important to select elastic scattering events, rejecting background from radiative or elastic process and to minimize systematic effects in the determination of t. Note that for scattering angles between ~ 2 and ~ 3 mrad there is an ambiguity between the outgoing electron and muon, as their angles and momenta are similar, to be resolved by means of μ/e discrimination.

(*v*) The boosted kinematics allows the same detector to cover the whole acceptance. Many systematic errors, *e.g.* on the efficiency, will cancel out (at least at first order) in the relative ratios of event counts in the high and low q^2 regions (signal and normalization regions). [13]

2.3 The experimental apparatus

The goal of the experiment is to precisely measure the shape of the differential cross section of the $\mu + e \longrightarrow \mu + e$ elastic scattering. The experiment has fixed-target layout, in which a muon beam (with momentum $\simeq 150$ GeV, from the CERN M2 muon beamline) impinge on the atomic electrons of Beryllium targets. The measures of the ougoing angles of the particles, after the scattering event, are performed by tracking detectors. Therefore, the multiple Coulomb scattering has to be minimized in order to achieve the best resolution possible. The total target thickness of 60 cm, required to collect the necessary statistic in a resonable running time, is divided into 40 modules each one composed by a target layer (15 mm of Beryllium) and several tracking stations, with lever arm of about 1 m.

In the apparatus is present an electromagnetic calorimeter (ECAL), placed downstream all stations. This calorimeter allow to do the particle identification and the measurement of the electron energy.

Should the contamination of pions in the muon beam be not low enough, a muon filter, instrumented with a muon chambers, will be added to the apparatus, downstream ECAL.

We present a schematic view of the experimental apparatus in Fig. 2.4. [14]

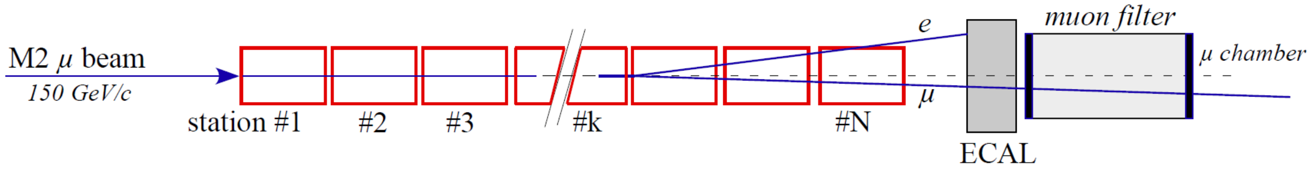

Figure 2.4: Schematic view of the MUonE experimental apparatus (not to scale).

2.3.1 Tracking system

The heart of the MUonE detector is the tracking system, which provide a precise measurement of the scattering angles of the outcoming muon and electron with respect to the initial direction of the muon beam. The region of full efficiency for the detector correspond to an electron energy greater than 1 GeV. The muon initial energy in the beam is about 150 GeV, therefore the maximum scattering angle for the electron is about 30 mrad. It is sufficient to cover an area of about 10×10 cm^2 with the tracking system to include all the kinematics of the event.

By recalling the modular structure of the detector, it is possible to see another feature of the MUonE experiment: the muon beam is reusable along the stations. This feature allows to increase the statistic of μe events, limiting at the same time the longitudinal lenght of the target, with the advantage of greatly reducing multiple scattering, at the same total event rate. Tracking between two targets provides the meaure for the particle angles and the direction of the beam for the next target. This modularity requirement implies a length of approximately one meter for each station, together with a target thickness of 15 mm of Be, in order to keep a reasonable total length of the apparatus.

There are some requirements related to the detector angular resolution. The angular information allows to distinguish muons from electrons using solely the angular information, with the exception of a limited ambiguity region, which is determined by the the angular resolution itself.

We show in Fig. 2.6 the distribution of two measured scattering angles, θ_{left} and θ_{right}. It is shown for events simulated with different angular resolutions. Here θ_{left} and θ_{right} are the scattering angles selected randomly, without particle identification. The ambiguity region becomes greater with the increasing of the detector resolution, from the ideal case, with only the multiple scattering from the target. An additional motivation for high angular resolution is an accurate definition of the signal region. Other scattering events with a photon in the final state ($\mu e \to \mu e \gamma$) do not follow the elastic curves show in Fig. 2.6 and need to be either identified with the calorimeter or rejected by means of angular cuts. The angular resolution is related to the spatial resolution of the tracker planes, orthogonal to the direction of the beam: an angular resolution of 0.02 mrad over one meter length corresponds to a spacial resolution of 20 μm, which can be achieved

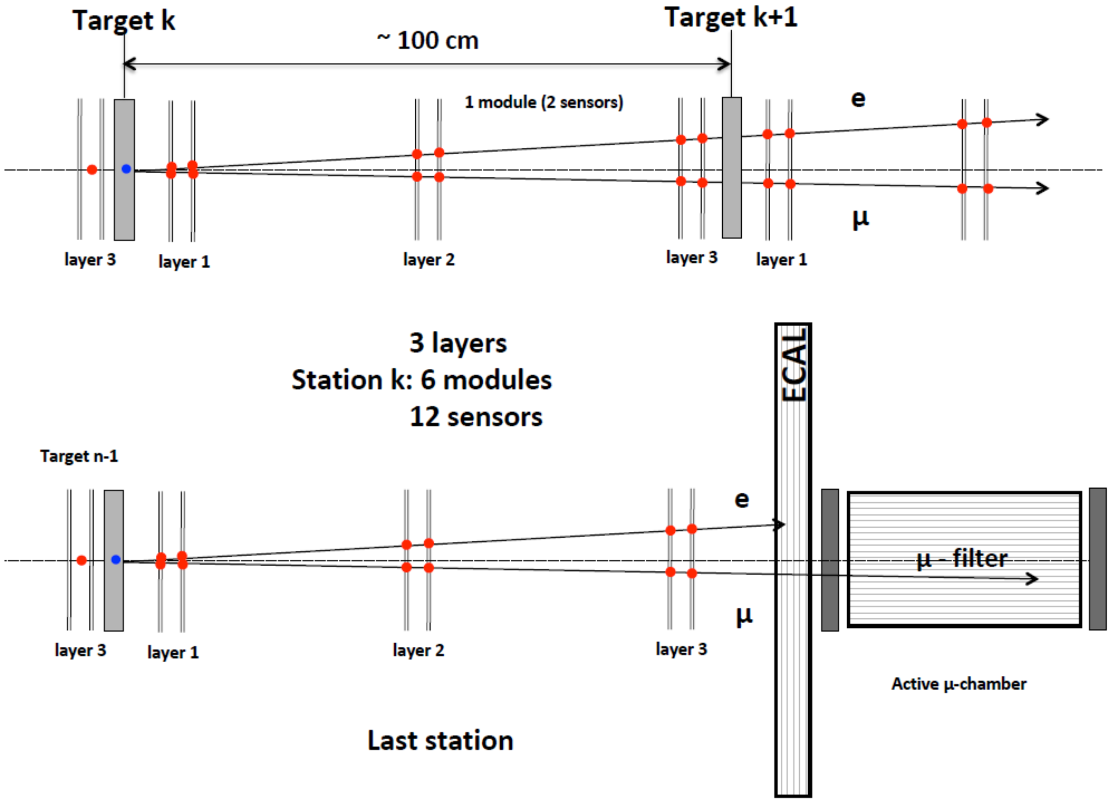

Figure 2.5: (upper) A sketch of one station, which is repeated 40 times in the final apparatus. (lower) Representation of the last station, which is followed by the calorimeter and the muon filter (not to scale).

with state-of-the-art Silicon detectors.

Silicon detector have a high signal-to-noise ratio ($S/N \simeq 25$), can achieve a detection close to 100% and sustain high rate (70 MHz). Therefor can satisfy the requirements of the beam. In addition the required coverage of 30 mrad can be achieved with a single Silicon sensor over a distance of 1 m with a state-of-the-art tecnology, ensuring an active area over the full detector.

The minimum requirement for the track determination is to have two sensitive planes, each mesuring a coordinate orthogonal to the beam direction (x,y). For Silicon strip detectors each plane must include two sensor to measure the x and the y coordinates. To improve the measure and the tracking efficiency from data themselves, a third plane is added, making a total of six sensors in three planes for each station.

As multiple scattering is an important source of systematic uncertainty in MUonE, it is also desirable to avoid additional detectors, solely dedicated to triggering. In this sense Silicon sensor have the advantage, over other tracking detector, that can provide trigger capabilities, if equipped with proper electronics.

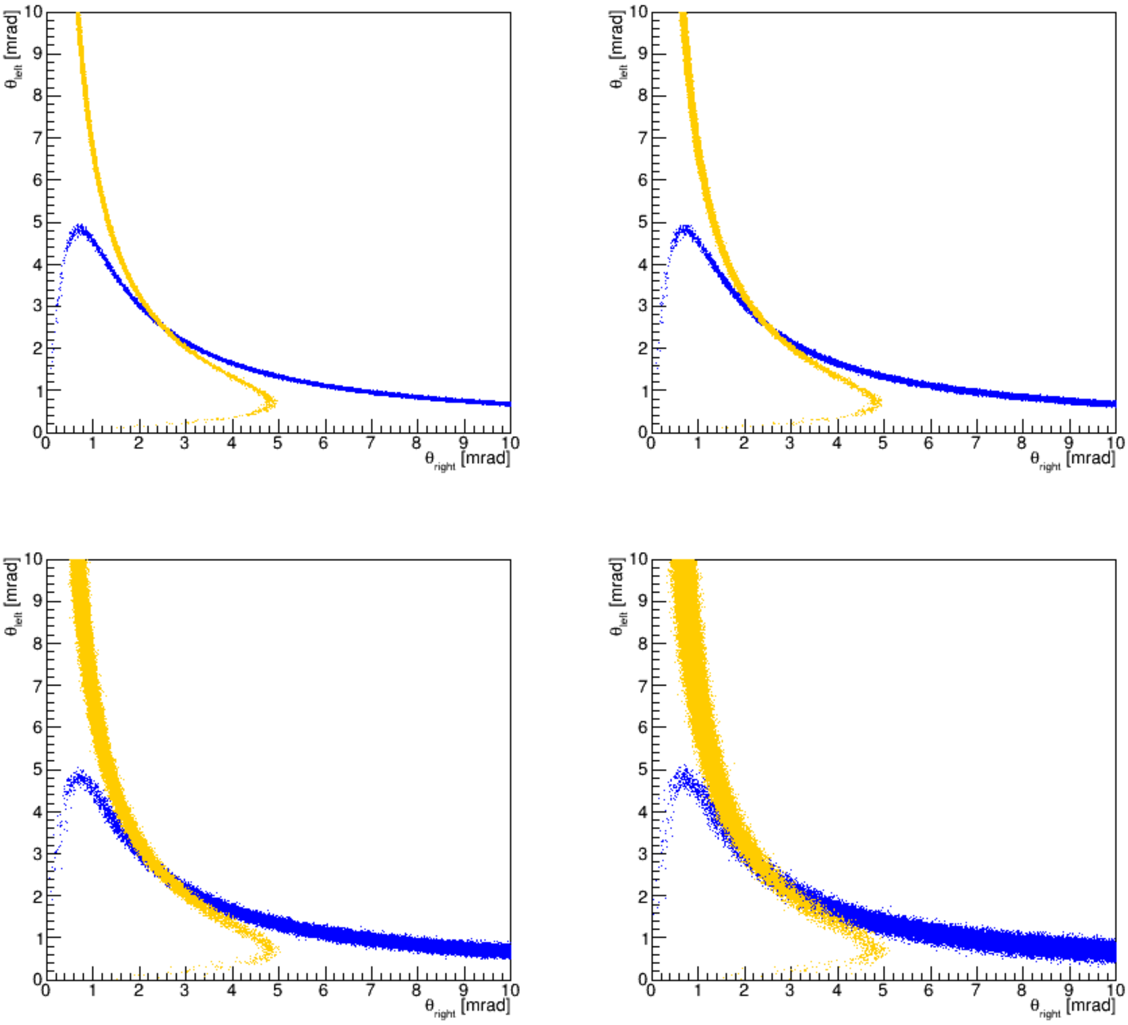

Figure 2.6: Distribution of the two measured scattering angles, θ_{left} versus θ_{right}: (top left) for events simulated with ideal angular resolution (only multiple scattering from the target included), (top right) angular resolution of 0.02 mrad, (bottom left) 0.06 mrad and (bottom right) 0.1 mrad, respectively. In blue are the points corresponding to the correct particle identification, in yellow the wrong identification.

Silicon sensor: the CMS module

The development of new Silicon sensors, with the necessary front-end readout electronics, requires a few years. Choosing among existing sensors, already designed for current experiments, represents a convenient hypothesis.

The Silicon strip sensor being produced for the CMS tracker upgrade feature a large active area. A single CMS sensor can cover the full angular acceptance for the MUonE purpose, and have an adeguate spacial resolution. It can also sustain the 40 MHz readout rate required for MUonE, with their accompanying front-end electronics. It can provide the track-trigger and also represent a good compromise for the detector thickness.

The Silicon sensor forseen for the CMS HL-LHC Outer Tracker (OT) is 320 μm thick sensor with n-in-p polarity produced by Hamamatsu Photonics (HPK). The sensor considered for MUonE is designed for the so-called 2S modules of the CMS OT, which is a square sensor with an area of 10 cm × 10 cm. The strips are capacitively-coupled, with a pitch of 90 μm and are segmented in two approximately 5 cm long strips. At each side of the sensor 1016 strips are read out by eight ASIC chips (CMC Binary Chips, CBC), for a total of 2032 channels.

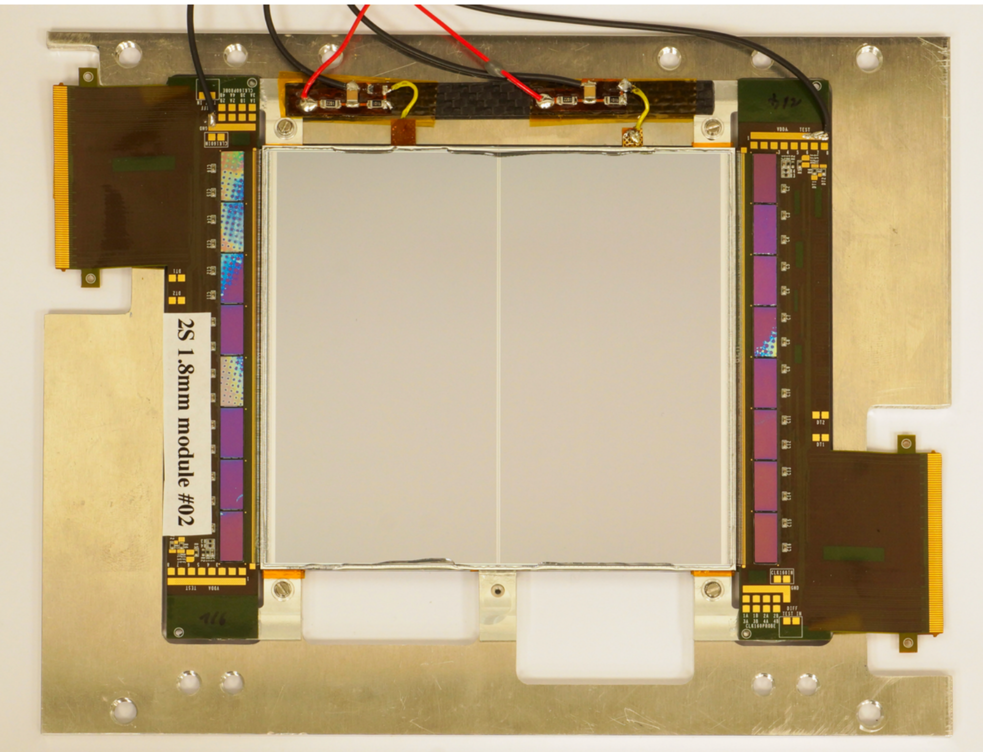

Figure 2.7: A picture of the CMS 2S module.

Chapter 3

Simulation of the $\mu + e \longrightarrow \mu + e$ event

3.1 $\mu + e \to \mu + e$ cross section

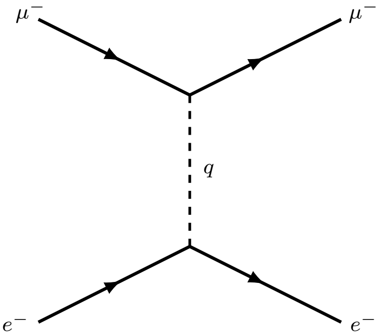

Figure 3.1: Tree level Feynman diagram for the μe scattering process.

The $\mu + e \to \mu + e$ scattering cross section is evalutated in the Born approximation. By applying the Feynman rules to the scattering process in the t-channel (shown in Fig. 3.1), assuming as incoming states an electron with 4-momentum p_e and spinor index s_e, and muon with 4-momentum p_μ and spinor index s_μ; and as outgoing states an electron with 4-momentum p'_e and spinor index s'_e and a muon with 4-momentum p'_μ and spinor index s'_μ. The matrix element is given by:

$$\mathcal{M}_{s_e,s'_e,s_\mu,s'_\mu} = \bar{u}_{s'_e}(p'_e)(-e\gamma^\mu)u_{s_e}(p_e)D_{\mu\nu}\bar{u}_{s'_\mu}(p'_\mu)(-e\gamma^\nu)u_{s_\mu}(p_\mu). \tag{3.1}$$

Summing up over the spin indices, the square modulus of the matrix element becomes:

$$
\begin{aligned}
&|\mathcal{M}(p_e, p'_e, p_\mu, p'_\mu)|^2 = \frac{1}{4}\sum_{s_e, s'_e}\sum_{s_\mu, s'_\mu} |\mathcal{M}_{s_e, s'_e, s_\mu, s'_\mu}(p_e, p'_e, p_\mu, p'_\mu)|^2 \\
&= \frac{1}{4}\sum_{s_e, s'_e}\sum_{s_\mu, s'_\mu} \frac{e^4}{(p'_e - p_e)^4} g_{\mu\nu} g_{\rho\sigma} (\bar{u}_{s'_e}(p'_e)\gamma^\mu u_{s_e}(p'_\mu)\bar{u}_{s'_\mu}(p'_\mu)\gamma^\nu u_{s_\mu}(p_\mu)) \\
&\times (\bar{u}_{s_e}(p_e)\gamma^\rho u_{s'_e}(p'_e)\bar{u}_{s_\mu}(p_\mu)\gamma^\sigma u_{s'_\mu}(p'_\mu)).
\end{aligned}
\tag{3.2}
$$

Using the completeness relation in general

$$\sum_s u_s(p) \otimes \bar{u}_s(p) = (\not{p} + m) \tag{3.3}$$

follows

$$|\mathcal{M}(p_e, p'_e, p_\mu, p'_\mu)|^2 = \frac{e^4}{4t^2} g_{\mu\nu} g_{\rho\sigma} \mathrm{tr}[(\not{p}'_e + m_e)\gamma^\mu(\not{p}_e + m_e)\gamma^\rho]\mathrm{tr}[(\not{p}'_\mu + m_\mu)\gamma^\nu(\not{p}_\mu + m_\mu)\gamma^\sigma] \tag{3.4}$$

where t represents the transferred momentum.

Considering terms with an even number of the γ^μ matrices (the trace of an odd number of γ is equal to zero) and computing the trace of two and four Dirac matrices it results:

$$\mathrm{tr} = 4g^{\mu\nu}; \tag{3.5}$$

$$\mathrm{tr} = 4(g^{\mu\nu}g^{\rho\sigma} - g^{\mu\sigma}g^{\mu\rho} + g^{\nu\rho}g^{\mu\sigma}). \tag{3.6}$$

Using the equation above, the matrix element can be written as:

$$
\begin{aligned}
&|\mathcal{M}(p_e, p'_e, p_\mu, p'_\mu)|^2 = \frac{4e^4}{t^2} g_{\alpha\beta} g_{\rho\sigma} (p'^{\alpha}_e p^{\rho}_e + p'^{\rho}_e p^{\alpha}_e + g^{\alpha\rho}(m^2_e - p'_e \cdot p_e)) \\
&\times (p'^{\beta}_\mu p^{\sigma}_\mu + p'^{\sigma}_\mu p^{\beta}_\mu + g^{\beta\sigma}(m^2_\mu - p'_\mu \cdot p_\mu)) \\
&= \frac{4e^4}{t^2}(p'_{e\beta} p_{e\sigma} + p'_{e\sigma} p_{e\beta} + g_{\beta\sigma}(m^2_e - p'_e \cdot p_e))(p'^{\beta}_\mu p^{\sigma}_\mu + p'^{\sigma}_\mu p^{\beta}_\mu + g^{\beta\sigma}(m^2_\mu - p'_\mu \cdot p_\mu)) \\
&= \frac{8e^4}{t^2}[(p'_e \cdot p'_\mu)(p_e \cdot p_\mu) + (p'_e \cdot p_\mu)(p_e \cdot p'_\mu) - m^2_\mu(p'_e \cdot p_e) - m^2_e(p'_\mu \cdot p_\mu) + 2m^2_e m^2_\mu].
\end{aligned}
\tag{3.7}
$$

It is useful to rewrite Eq. (3.7) as a function of the Mandelstan's variables:

$$\begin{aligned} s &= (p_e + p_\mu)^2 = m_e^2 + m_\mu^2 + 2p_e \cdot p_\mu; \\ t &= (p_e - p_e')^2 = 2m_e^2 - p_e \cdot p_e'; \\ u &= (p_e - p_\mu')^2 = m_e^2 + m_\mu^2 - 2p_e \cdot p_\mu'; \end{aligned} \tag{3.8}$$

and thereby

$$\begin{aligned} &(p_e \cdot p_\mu) = [p_e^2 + p_\mu^2 - (p_e + p_\mu)^2]/2 = (s - m_e^2 - m_\mu^2)/2 = (p_e' + p_\mu'); \\ &(p_e \cdot p_\mu') = (m_e^2 + m_\mu^2 - u)/2 = (p_e' \cdot p_\mu); \\ &(p_e \cdot p_e') = (2m_e^2 - t)/2; \\ &(p_\mu \cdot p_\mu') = (2m_e^2 - t)/2. \end{aligned} \tag{3.9}$$

The amplitude in Eq. (3.7) becomes

$$\begin{aligned} |\mathcal{M}(p_e, p_e', p_\mu, p_\mu')|^2 =& \frac{8e^4}{t^2}\Big[\frac{(s - m_e^2 - m_\mu^2)^2}{4} + \frac{(m_e^2 + m_\mu^2 - u)^2}{4} \\ & - m_\mu^2\Big(\frac{2m_e^2 - t}{2}\Big) - m_e^2\Big(\frac{2m_\mu^2 - t}{2}\Big) + 2m_e^2 m_\mu^2\Big]. \end{aligned} \tag{3.10}$$

Using the relation between the Mandelstan's variables

$$s + t + u = 2(m_e^2 + m_\mu^2) \tag{3.11}$$

we obtain the amplitude $|\mathcal{M}(p_e, p_e', p_\mu, p_\mu')|^2$ as a function of two of them:

$$\begin{aligned} |\mathcal{M}(s,t)|^2 =& \frac{8e^4}{t^2}\Big[\frac{(s - m_e^2 - m_\mu^2)^2}{4} + \frac{(s + t - m_e^2 - m_\mu^2)^2}{4} + \frac{tm_\mu^2}{2}\frac{tm_e^2}{2}\Big] \\ =& \frac{2e^4}{t^2}(t^2 + 2st + 2s^2 - 4sm_e^2 - 4sm_\mu^2 + 2m_\mu^4 + 2m_\mu^4 + 4m_e^2 m_\mu^2), \end{aligned} \tag{3.12}$$

which may be written as

$$|\mathcal{M}(s,t)|^2 = \frac{4e^4}{t^2}\Big(\frac{t^2}{2} + st + (s - m_\mu^2 - m_e^2)^2\Big). \tag{3.13}$$

The differential cross section is given by

$$d\sigma = \frac{(2\pi)^4 |\mathcal{M}|^2}{4\sqrt{(p_e \cdot p_\mu)^2 - m_\mu^2 m_e^2}} \times d\Phi(p_e + p_\mu; p_e', p_\mu'). \tag{3.14}$$

where $d\Phi$ is the element of the phase space and is given by

$$d\Phi(p_e + p_\mu, p'_e, p'_\mu) = \delta^4(p_e + p_\mu - p'_e - p'_\mu)\frac{dp'_e}{(2\pi)^3 2E'_e}\frac{dp'_\mu}{(2\pi)^3 2E'_\mu}. \tag{3.15}$$

In the rest frame of m_e,

$$\sqrt{(p_e \cdot p_\mu)^2 - m_e^2 m_\mu^2} = m_e p_\mu. \tag{3.16}$$

Using Mandelstan's variables, the differential cross section in the variable t may be written as

$$\frac{d\sigma}{dt} = \frac{1}{64\pi s}\frac{1}{|\mathbf{p}_{cm}|^2}|\mathcal{M}|^2. \tag{3.17}$$

From the relativistic kinematics, the definition of $p_{\mu,cm}$ in the center of mass frame is

$$|p_{\mu,cm}| = \frac{\sqrt{\lambda(s, m_\mu^2, m_e^2)}}{2\sqrt{s}}, \tag{3.18}$$

where $\lambda(s, m_\mu^2, m_e^2)$ is the Kallen function, defined in Eq. (A.8). The Eq. (3.18) can be used in Eq. (3.17):

$$\frac{d\sigma}{dt} = \frac{1}{64\pi}\frac{4}{\lambda(s, m_\mu^2, m_e^2)}|\mathcal{M}|^2. \tag{3.19}$$

Finally, using the amplitude found in the Eq. (3.13), the Eq. (3.17) can be written as

$$\frac{d\sigma}{dt} = \frac{4\pi\alpha^2}{\lambda(s, m_\mu^2, m_e^2)}\Big[\frac{(s - m_\mu^2 - m_e^2)^2}{t^2} + \frac{s}{t} + \frac{1}{2}\Big] \tag{3.20}$$

3.1.1 Differential cross section in the electron angle

Now, the differential cross section can be found as function of the outcoming electron angle θ_e, using the relation

$$\frac{d\sigma}{d\theta_e} = \frac{d\sigma}{dt}\left|\frac{dt}{d\theta_e}\right|. \tag{3.21}$$

In order to have a relation between the variable t and the angle θ_e it is necessary to found the energy of the electron $E'_e = E'_e(\theta_e)$. Assuming

$$\begin{aligned} p_\mu &= (E_\mu, p_\mu, 0, 0);\\ p_e &= (m_e, 0, 0, 0) :\\ p'_\mu &= (E_\mu + m_e - E'_e, p'_e \cos\theta_\mu, p'_e \sin\theta_e, 0);\\ p'_e &= (E'_e, p'_e \cos\theta_e, -p'_e \sin\theta_e, 0); \end{aligned} \tag{3.22}$$

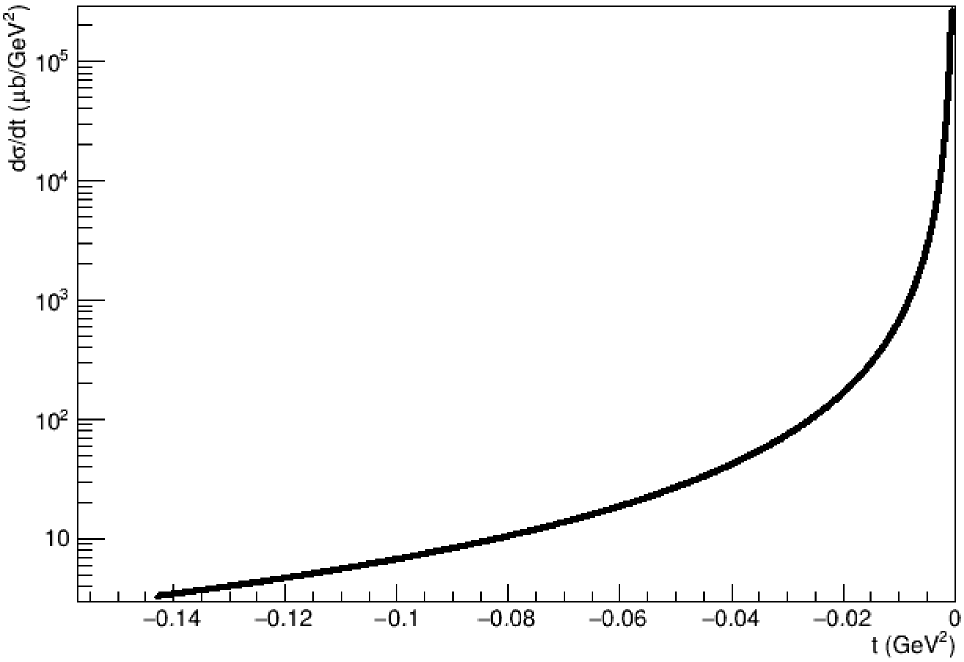

Figure 3.2: $\frac{d\sigma}{d\theta_e}$ as function of θ_e.

the product of the 4-momenta is

$$m_e^2 + m_e E_\mu - E_\mu E'_e + p_\mu p'_e \cos\theta_e - m_e E'_e = 0. \tag{3.23}$$

With the mass-shell relation

$$p_\mu \sqrt{E'_e - m_e} \cos\theta_e = (E'_e - m_e)(E_\mu m_e) \tag{3.24}$$

from which

$$p_\mu^2 cos^2\theta_e (E'_e - m_e)(E'_e + m_e) = (E'_e - m_e)(E_\mu m_e) \tag{3.25}$$

and then

$$E'_e = m_e \frac{(E_\mu + m_e)^2 + p_\mu^2 \cos^2\theta_e}{(E_\mu + m_e)^2 - p_\mu^2 \cos^2\theta_e}. \tag{3.26}$$

Finally, using

$$r = \frac{\sqrt{(E_\mu^2 - m_\mu^2)}}{E_\mu + m_e} \tag{3.27}$$

the final energy of the electron can be written as

$$E'_e = m_e \frac{1 + r^2 \cos^2\theta_e}{1 - r^2 \cos^2\theta_e}. \tag{3.28}$$

The relation between the tranferred momentum and the scattering angle of the electron is then:

$$\begin{aligned} t &= 2m_e^2 - 2m_e E'_e \\ &= 2m_e\Big(1 - \frac{1 + r^2\cos^2\theta_e}{1 - r^2\cos^2\theta_e}\Big) \\ &= \frac{4m_e^2 r^2 \cos^2\theta_e}{r^2\cos^2\theta_e - 1}. \end{aligned} \tag{3.29}$$

This lends to the final form of the differential cross section in the variable θ_e. From the Eq. (3.21), and differentiating the Eq. (3.29),

$$\frac{d\sigma}{d\theta_e} = \frac{8m_e^2 r^2 \cos\theta_e \sin\theta_e}{(r^2\cos^2\theta_e - 1)^2} \frac{d\sigma}{dt} \tag{3.30}$$

3.1.2 Differential cross section in the muon angle

In order to obtain the differential cross section as function of the the variable θ_μ it is useful to rewrite the incoming and outgoing particle 4-momenta:

$$\begin{aligned} p_e &= (m_e, 0, 0, 0); \\ p_\mu &= (E_\mu, p, 0, 0); \\ p'_e &= (E'_e, p'\cos\theta_e, p'\sin\theta_e, 0); \\ p'_\mu &= (E'_\mu, p'\cos\theta_\mu, p'\sin\theta_\mu, 0). \end{aligned} \tag{3.31}$$

Using the 4-momentum conservation, we write

$$p'_e = p_e + p_\mu - p'_\mu \tag{3.32}$$

which squared becomes

$$0 = m_\mu^2 + p_e p_\mu - p_e p'_\mu - p_\mu p'_\mu. \tag{3.33}$$

Rewriting the products in the relation above

$$\begin{aligned} p_e p_\mu &= m_e E_\mu; \\ p_e p'_\mu &= m_e E_\mu; \\ p_\mu p'_\mu &= E_\mu E'_\mu - p_\mu p'_\mu \cos\theta_\mu. \end{aligned} \tag{3.34}$$

The Eq. (3.33) can be rewritten as

$$\begin{aligned} 0 &= m_\mu^2 + m_e E_\mu - m_e E'_\mu - E_\mu E'_\mu + p_\mu p'_\mu \cos\theta_\mu \\ &= m_\mu^2 + m_e\big(E'_e - m_e\big) - E_\mu\big(E_\mu + m_e - E'_e\big) + p_\mu p'_\mu \cos\theta_\mu, \end{aligned} \tag{3.35}$$

where the energy conservation was used in the second line. From the relation above it is possible to write:

$$\cos\theta_\mu = \frac{E_\mu^2 + E_\mu m_e - E_\mu E'_e - m_e E'_e + m_e^2 - m_\mu^2}{\sqrt{E_\mu^2 - m_\mu^2}\sqrt{(E_\mu + m_e - E'_e)^2 - m_\mu^2}}. \tag{3.36}$$

In this equation the scattered electron energy can be found, but, in order to obtain the differential cross section it is necessary to rewrite it with the Mandelstam variable t instead of E'_e. Using the definition of t

$$t = (p_e - p'_e)^2 = 2m_e^2 - 2m_e E'_e \tag{3.37}$$

from which we get

$$E'_e = m_e - \frac{t}{2m_e}. \tag{3.38}$$

Using the latter in the Eq. (3.36) may be written as

$$\cos\theta_\mu = \frac{E_\mu^2 + E_\mu t/(2m_e) - t/2 - m_\mu^2}{\sqrt{E_\mu^2 - m_\mu^2}\sqrt{E_\mu^2 + t/(4m_e^2) + E_\mu t/m_e - m_\mu^2}}. \tag{3.39}$$

This relation can be inverted in order to write t as a function of the angle θ_μ

$$\begin{aligned} 0 =& t^2\left[p_\mu^2 \cos^2\theta_\mu - (E_\mu + m_e)^2\right] + \\ &+ 4m_e p_\mu^2 t(E_\mu \cos^2\theta_\mu - E_\mu - m_e) + \\ &+ 4m_e^2 p_\mu^4(\cos^2\theta_\mu - 1) \end{aligned} \tag{3.40}$$

where $p_\mu = \sqrt{E_\mu^2 - m_\mu^2}$.

In the first two terms of the Eq. (3.40) we find the initial energy $E_\mu + m_e$, which, in the considered scenario, can be defined as

$$E \equiv E_\mu + m_e \simeq 150 \text{ GeV}. \tag{3.41}$$

The Eq. (3.40) may be written as

$$(p_\mu^2 \cos^2\theta_\mu - E)t^2 + 4m_e p_\mu^2 (E_\mu \cos^2\theta_\mu - E)t + 4m_e^2 p_\mu^4 (\cos^2\theta_\mu - 1) = 0. \tag{3.42}$$

The two solutions for the latter are

$$t_\pm = 2m_e p_\mu^2 \frac{-E_\mu \cos^2\theta_\mu + E \pm \sqrt{(E_\mu \cos^2\theta_\mu - E)^2 - (p_\mu^2 \cos^2\theta_\mu - E^2)(\cos^2\theta_\mu - 1)}}{p_\mu^2 \cos^2\theta_\mu - E^2}. \tag{3.43}$$

Solving term in the square root

$$\begin{aligned} &(E_\mu \cos^2\theta_\mu - E)^2 - (p_\mu^2 \cos^2\theta_\mu - E^2)(\cos^2\theta_\mu - 1) = \\ &= (E_\mu^2 - p_\mu^2)\cos^4\theta_\mu + (E^2 + p_\mu^2 - 2EE_\mu)\cos^2\theta_\mu = \\ &= m_\mu^2 \cos^4\theta_\mu + (m_e^2 - m_\mu^2)\cos^2\theta_\mu. \end{aligned} \tag{3.44}$$

Therefore the Eq. (3.43) becomes

$$t_\pm = 2m_e(E_\mu^2 - m_\mu^2) \frac{m_e + E_\mu(1 - \cos^2\theta_\mu) \pm \sqrt{[m_\mu^2(\cos^2\theta_\mu - 1) + m_e^2]\cos^2\theta_\mu}}{(E_\mu^2 - m_\mu^2)\cos^2\theta_\mu - (E_\mu + m_e)^2}. \tag{3.45}$$

The Mandelstam variable t is negative in the experimental framework considered. Then it is necessary to choose which solution is correct.

The denominator is negative

$$(E_\mu^2 - m_\mu^2)\cos^2\theta_\mu - (E_\mu + m_e)^2 < 0 \tag{3.46}$$

due to

$$(E_\mu^2 - m_\mu^2) < E_\mu^2, \tag{3.47}$$

which implies

$$(E_\mu^2 - m_\mu^2)\cos^2\theta_\mu < E_\mu^2, \tag{3.48}$$

while

$$(E_\mu^2 + m_e^2)^2 > E_\mu^2. \tag{3.49}$$

The numerator is written as

$$m_e + E_\mu(1 - \cos^2\theta_\mu) \pm \sqrt{[m_\mu^2(\cos^2\theta_\mu - 1) + m_e^2]\cos^2\theta_\mu} > 0, \tag{3.50}$$

this inequality is true indipendently from the sign of the square root. The latter exist in the interval

$$0 \leq \sqrt{[m_\mu^2(\cos^2\theta_\mu - 1) + m_e^2]\cos^2\theta_\mu} \leq m_e \tag{3.51}$$

because $1 - (m_e/m_\mu)^2 \leq \cos^2\theta_\mu \leq 1$.

We understand that we cannot determine the right solution in this way because both are less than zero. It is known that the variable t, in this scattering scenario, can have values in a range

$$(-0.142893 \leq t \leq 0)\ \mathrm{GeV}^2 \tag{3.52}$$

Therefore, in the plane $\cos^2\theta_\mu - t$ (with the cosine on the x-axis and the Mandelstam variable on the y-axis) it is allowed to assume that only one solution lays on the IV quadrant ($t < 0$) with limits:

$$0.999976609 \leq \cos^2\theta_\mu \leq 1, \tag{3.53}$$

which correspond to

$$(-0.142893 \leq t \leq 0)\ \mathrm{GeV}^2. \tag{3.54}$$

This assumption is not wrong: studying the limits of the two solutions for $\theta_\mu \to 0.999976609^+$ we observe that t_+ comes from the infinite, while t_- comes from zero (in effect $t_-(\cos\theta_\mu = 1) = 0$). Now it is necessary to calculate the derivative of $t_-(\cos\theta_\mu)$. The variable t is then rewritten in the form

$$t_- = 2m_e p_e^2 \frac{m_e + E_\mu \sin^2\theta_\mu - \sqrt{[m_e^2 - m_\mu^2 \sin^2\theta_\mu]\cos^2\theta_\mu}}{p_\mu^2\cos^2\theta_\mu - E^2}. \tag{3.55}$$

The derivative of t_- is:

$$\begin{aligned}\frac{dt_-}{d\theta_\mu} =& \frac{2m_e p_\mu^2}{p_\mu^2\cos^2\theta_\mu - E^2}\left[2E_\mu\cos\theta_\mu\sin\theta_\mu + \frac{m_\mu^2\cos^3\theta_\mu\sin\theta_\mu + [m_e^2 - m_\mu^2\sin^2\theta_\mu]\cos\theta_\mu\sin\theta_\mu}{\sqrt{[m_e^2 - m_\mu^2\sin^2\theta_\mu]\cos^2\theta_\mu}}\right] + \\ &+ \frac{2m_e p_\mu^2}{p_\mu^2\cos^2\theta_\mu - E^2}\left[\frac{m_e + E_\mu\sin^2\theta_\mu - \sqrt{[m_e^2 - m_\mu^2\sin^2\theta_\mu]\cos^2\theta_\mu}}{p_\mu^2\cos^2\theta_\mu - E^2}(p_\mu^2\cos\theta_\mu\sin\theta_\mu)\right]\end{aligned} \tag{3.56}$$

Chapter 4

Reconstruction of the initial energy

The physical process we are considering is the elastic scattering $\mu + e \to \mu + e$. The muon energy is $E_\mu = 150$ GeV. They will hit electrons at rest in the Beryllium target.

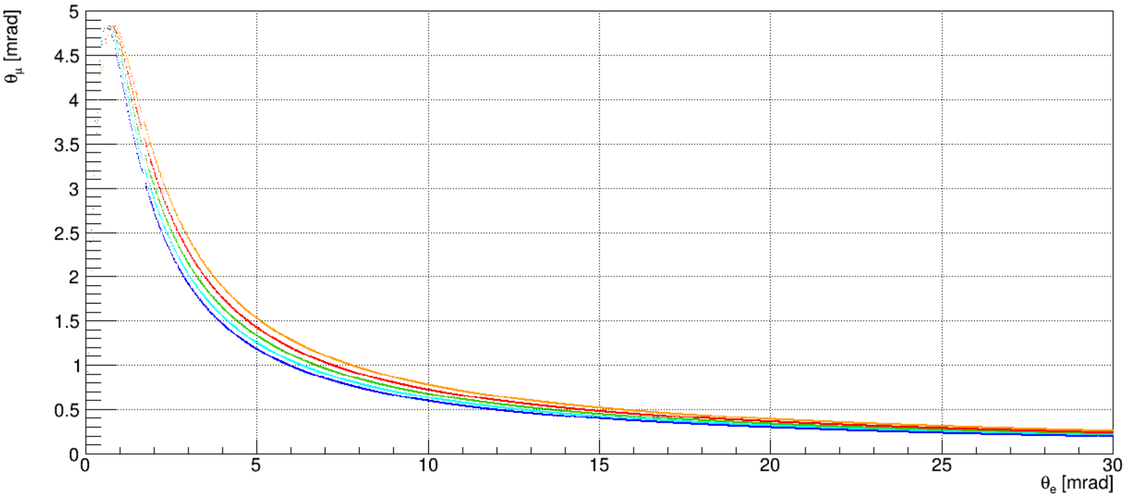

Figure 4.1: The $\theta_e - \theta_\mu$ angular relation for the elastic scattering at different energies. The blue dots corresponds to a muon energy of 130 GeV, light blue to 140 GeV, green to 150 GeV, red to 160 GeV, yellow to 170 GeV.

In order to determine $\alpha(t)$, we aim to get an accurate measure of the shape of the cross section $d\sigma/dt$. On this purpose it is necessary to know the initial muon energy with high precision, of the order of few MeV.

From the scattering theory we know the cross section (leading order) of this event and we can use Mandelstam's variables to write it as:

$$\frac{d\sigma}{dt} = \alpha(t)\frac{d\sigma_0}{dt}(t,s), \tag{4.1}$$

where we distinguish the kinematic contribution $\frac{d\sigma_0}{dt}(t,s)$ from the interaction coupling $\alpha(t)$. We want to calculate the cross section $\frac{d\sigma_0}{dt}(t,s)$ using the most accurate value of s. It implies that we need an accurate measure of the muon initial energy E_μ.

The detector is made up by many stations, which are located one downstream the other. Each station is provided with a target and tracking system. Therefore each station, beacuse of the material budget, cause an non negligible energy loss. We know that 1.5 cm of Beryllium corresponds to

$$1.5 \text{ cm}/35.28 \text{ cm} = 0.04252\ X_{0,Be} \tag{4.2}$$

where $X_{0,Be} = 35.28$ cm $= 65.19$ g cm^2 is the Beryllium radiation length. A 150 GeV muon has an energy loss of ~ 2.5 MeV cm^2/g^{-1}. In our case the expected mean energy loss is (see appendix C)

$$\frac{dE}{dx} \simeq 2.5 \times 0.0452 \times X_{0,Be} \simeq 6.5 \text{ MeV}. \tag{4.3}$$

To perform the measure of a_μ^{HLO} it is necessary to know the mean energy of the incoming muon with a precision of few MeV, and it is important to have the best mean estimate for each station. To get the energy mean value we can rely on the tracking system, that is the only detector available in a station.

4.1 Kinematics used in the simulation of the event

The simulation of the events begin with the generation of a gaussian-distributed set of initial energies for the muon. The mean value is set to 150 GeV and the standard deviation to 150 × 0.0375 = 5.625 GeV, as the CERN M2 muon beam.

By knowing the muon energy E_μ we calculate s as:

$$s = m_e^2 + m_\mu^2 + 2m_eE_\mu. \tag{4.4}$$

We can then vary t betweeen t_{min} and t_{max} (as said in Eq. (3.52)) and calculate the differential cross section in the variable t and s, as in Eq. (3.20):

$$\frac{d\sigma}{dt} = \frac{4\pi\alpha^2}{\lambda(s,m_1^2,m_2^2)}\left[\frac{(s-m_\mu^2-m_e^2)^2}{t^2} + \frac{s}{t} + \frac{1}{2}\right] \tag{4.5}$$

We use these values to fill a histogram as function of t and s. From this histogram (shown Fig. 4.2) we can obtain the random values for E_μ and t according to their probability (the probability to happen is related to the cross section). By knowing s and t we

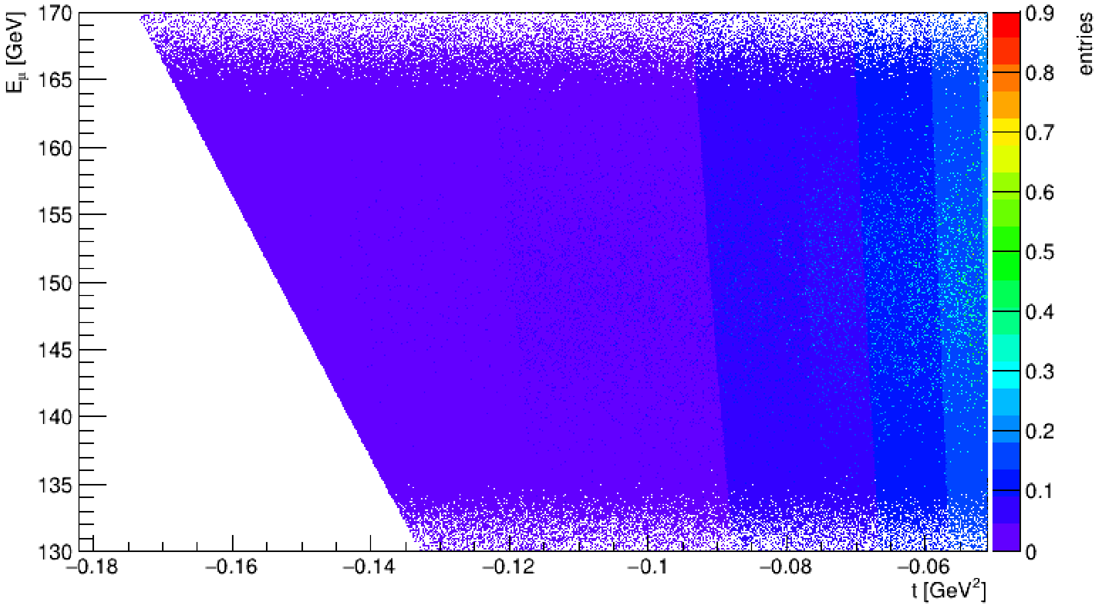

Figure 4.2: Initial energy E_μ as function of Mandelstam variable t weighted with the value of the cross section $d\sigma/dt$.

can reconstruct the elastic event. Using the relations from relativistic mechanics (see appendix A, Eqs. (A.15) and (A.14)), we can obtain θ_e and θ_μ. We recall the equation:

$$\cos\theta_e = \frac{E_\mu + me}{\sqrt{E_\mu^2 - m_\mu^2}}\sqrt{\frac{E'_e - m_e}{E'_e + m_e}}. \tag{4.6}$$

From the energy conservation $E'_\mu = E_\mu + m_e - E'_e$ and the moment conservation $p_\mu \sin\theta_\mu = p_e \sin\theta_e$ we obtain

$$\sin\theta_\mu = \frac{\sqrt{E'^2_e - m_e}}{\sqrt{E'^2_\mu - m_\mu}}\sin\theta_e. \tag{4.7}$$

We do consider the conditio where $\theta_e \simeq \theta_\mu$, so we focus in the angular region where the two particle angles are not distinguishable. In this case we can construct a kinematic variable to invert the Eq. (4.7) and reconstruct E_μ. This is shown in the representation of the relation between the scattering angle for different energies in Fig. 4.1. Different initial energies cause different shapes in the relation $\theta_e - \theta_\mu$, in particular in the region where $\theta_e \simeq \theta_\mu$, around 2-3 mrad.

Therefore, in order to satisfy the relation $\theta_e \simeq \theta_\mu$ we limited the simulation to the angles included in the interval between 2 and 3 mrad. We define then the distribution of the mean angle, θ_s.

$$\theta_s = \frac{1}{2}(\theta_\mu + \theta_e); \tag{4.8}$$

We can use this observable to reconstruct the initial energy.

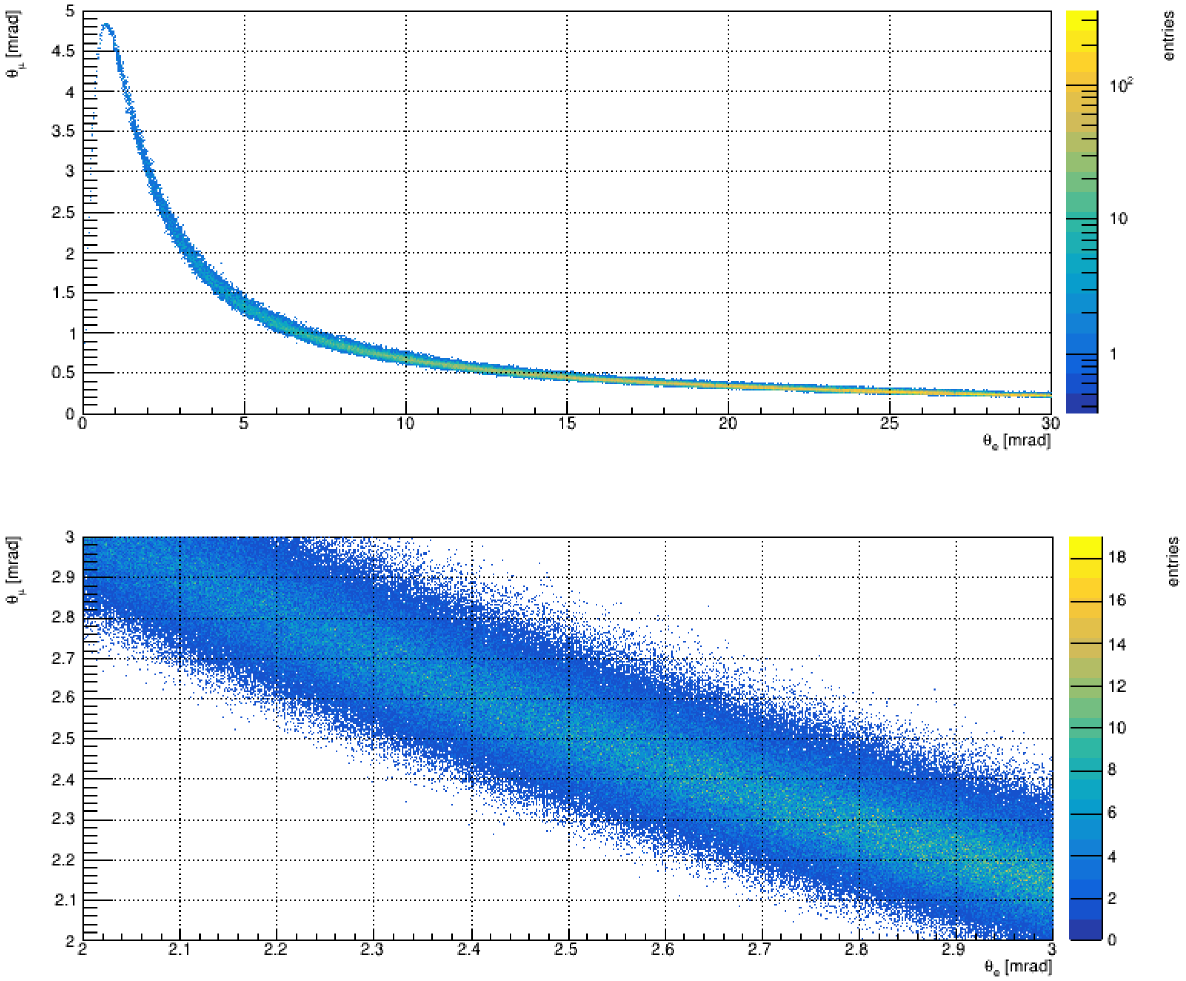

Figure 4.3: (top) Distribution of the θ_μ and θ_e angles for the initial muon energy of $E_\mu = 150.000 \pm 5.625$ GeV. (bottom) The same distribution in the interval between 2 mrad and 3 mrad.

4.2 Interaction with the apparatus

To get a realistic description of the detector effects it is necessary to simulate the passage of the particles through the detector material. We consider the passage through the target, extracting the collision vertex uniformly within the 1.5 cm Beryllium layer, and through four 600 μm thick Silicon layers.

In the previous section we described how to obtain an elestic event, according to the kinematics and without multiple scattering and detector resolution effects. At the stage the fluctuating quantities are the initial muon energy and the transferred momentum t. Subsequently θ_e and θ_μ are subjected to the smearing caused by the propagation through the matter and by the detector resolution.

There are three main sources of uncertainty acting on the angular variables: (i) The target is made of a 1.5 cm thick Beryllium layer. The path of the particles from the vertex to the surface of the Beryllium target is affected by the multuple scattering. (ii) The multiple scattering due to the passage of the particle through the Silicon tracking stations. (iii) The detector layers have an intrinsic resolution in measuring the hit position (intrinsic hit resolution).

4.2.1 Interaction with the detector material

The scattering vertex inside the target is extracted from an uniform distribution between 0 and d, we call it d_{cross}. The path from d_{cross} to the target surface is subject to a deflection due to the multiple scattering, as shonw in Fig. 4.6.

From Eq. (B.2), described in the appendix, we can calculate the Moliere multiple scattering angles for μ and e, we call them θ_μ^M and θ_e^M respectively.

$$\theta_\mu^M = \frac{13.6MeV}{E'_\mu}\sqrt{\frac{t_{cross}}{X_{0,Be}}}\left[1+0.038\ln\left(\frac{t_{cross}}{X_{0,Be}}\right)\right], \tag{4.9}$$

$$\theta_e^M = \frac{13.6MeV}{E'_e}\sqrt{\frac{t_{cross}}{X_{0,Be}}}\left[1+0.038\ln\left(\frac{t_{cross}}{X_{0,Be}}\right)\right], \tag{4.10}$$

where $X_{0,Be} = 35.28$ cm is the Beryllium radiation length, E'_μ and E'_e are the μ and e energies after the interaction. We have made the approximation $\beta \simeq c$ that result in $\beta pc = E$. We can use these angles to emulate the effect of multiple scattering by gaussian distributions with mean value zero and standard deviation corresponding to the Moliere angle:

$$G_{\mu,e}(0,\sigma_{\mu,e}) = G_{\mu,e}(0,\theta_{\mu,e}^M) \text{ for } \mu \text{ and } e \text{ respectively.} \tag{4.11}$$

With these distributions it is possible to extract a random value for the multiple scattering angle for μ and e that we call δ_μ^0 and δ_e^0 respectively. Therefore, after the first

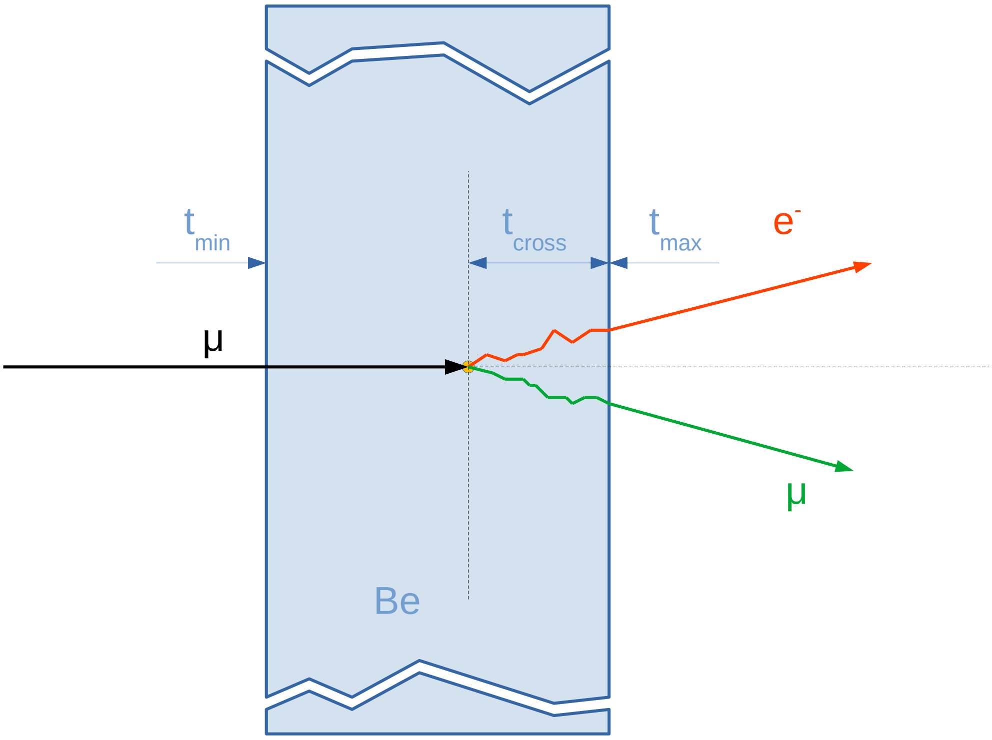

Figure 4.4: Representation of the multiple scattering in the path through the target. The standard of the angular distribution depends on the thickness and nature of the target, and on the particle energy.

multiple scattering process occurring in the target, we have new values of the muon and electron angles:

$$\begin{aligned} \theta_\mu^0 &= \theta_\mu + \delta_\mu^0, \\ \theta_e^0 &= \theta_e + \delta_e^0, \end{aligned} \tag{4.12}$$

where θ_μ and θ_e are the true scattering angles. Going through the detector particles reach the Silicon tracking stations, which cause further multiple scattering effects. We use the Eq. (B.2) again:

$$\theta_\mu^M = \frac{13.6MeV}{E'_\mu}\sqrt{\frac{d_1}{X_{0,Si}}}\left[1 + 0.038\ln\left(\frac{d_1}{X_{0,Si}}\right)\right], \tag{4.13}$$

$$\theta_e^M = \frac{13.6MeV}{E'_e}\sqrt{\frac{d_1}{X_{0,Si}}}\left[1 + 0.038\ln\left(\frac{d_1}{X_{0,Si}}\right)\right], \tag{4.14}$$

where $d_1 = 0.6$ mm is the Silicon layer thickness and $X_{0,Si} = 9.37$ cm is the Silicon radiation lenght. The same method procedure shown in Eq. (4.11) and Eq. (4.12) is used to simulate the effect of multiple scattering in the tracking station. We name δ_μ^1 and δ_e^1 the effect of layer 1 (that is the first layer downstream the target), δ_μ^2 and δ_e^2 the effect of layer 2, and so on. Therefore, for the four Silicon layers we have:

$$\begin{aligned}
\theta_{\mu,e}^1 &= \theta_{\mu,e} + \delta_{\mu,e}^0 + \delta_{\mu,e}^1;\\
\theta_{\mu,e}^2 &= \theta_{\mu,e} + \delta_{\mu,e}^0 + \delta_{\mu,e}^1 + \delta_{\mu,e}^2;\\
\theta_{\mu,e}^3 &= \theta_{\mu,e} + \delta_{\mu,e}^0 + \delta_{\mu,e}^1 + \delta_{\mu,e}^2 + \delta_{\mu,e}^3;\\
\theta_{\mu,e}^4 &= \theta_{\mu,e} + \delta_{\mu,e}^0 + \delta_{\mu,e}^1 + \delta_{\mu,e}^2 + \delta_{\mu,e}^3 + \delta_{\mu,e}^4.
\end{aligned} \tag{4.15}$$

These calculations are stored for each event of every simulation.

4.2.2 Tracking stations uncertainty

It is possible to measure the angle values shown in Eq. (4.15) within the detector intrinsic precision. In our case we are using Silicon strip tracker with a pitch of 90 μm. The intrinsic resolution of a hit position measurement is

$$\delta x = \frac{90}{\sqrt{2}\sqrt{12}} \sim 18\mu m. \tag{4.16}$$

From this we can calculate expected the angular resolution as:

$$\delta\theta_R \simeq \frac{\sqrt{2}\delta x}{L} \tag{4.17}$$

where L is the layer distance from the vertex. We name $\delta\theta_R$ the intrinsic angular resolution. This is a source of uncertainty that must be added to the multiple scattering. The error estimate for the layer 1 is then:

$$\delta\theta = \sqrt{c_0^2 + \left(\frac{c_1}{E}\right)^2} \tag{4.18}$$

where c_0 is the intrinsic resolution obtained in Eq.(4.17), and c_1 is the constant part of the Moliere formula for the Beryllium target that together with $1/E$ depenence represents

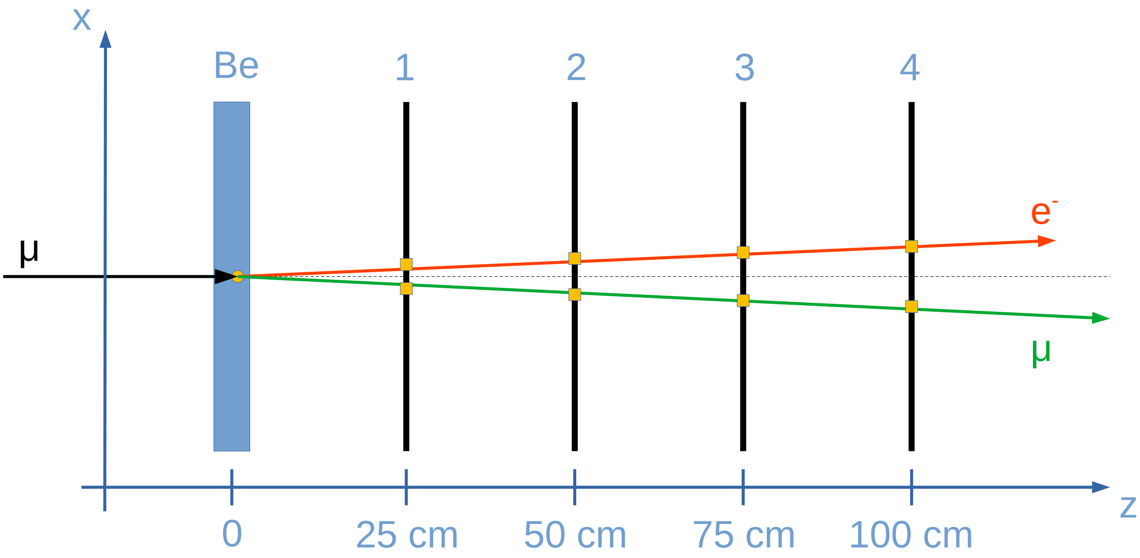

Figure 4.5: Detector layout. We simulate the passage through the target and four tracking stations.

the uncertainty due to the multiple scattering. Every tracking station has a different $\delta\theta$ due to the different position of the tracking stations downstream the target.

The outcoming paticle energies must be calculated from the knowledge of the angles and the muon initial energy E_μ. From the relativistic kinematics equations, we can calculate the electron energy after the event E'_e:

$$E'_e = m_e \frac{(E_\mu + m_e)^2 + (E_\mu^2 - m_\mu^2)\cos^2(\theta_\mu)}{(E_\mu + m_e)^2 - (E_\mu^2 - m_\mu^2)\cos^2(\theta_\mu)}. \tag{4.19}$$

We can make the approximation $E'_\mu \simeq E'_e$ since $\theta_\mu \simeq \theta_e$. Now we can use the Eq. (B.2) in order to obtain the term $(c_1/E)^2$ from Eq. (4.18). Therefore, independently from the particle nature (μ or e), we have an estimate for the single layer uncertainty.

Now we want to add the effect of the Silicon layer multiple scattering, we define the quantity c_2 that, similarly to c_1, is the constant part of the Moliere formula with the Silicon layer features. Finally it is possible to write the resolution for each layer:

$$\delta\theta^1_{e,\mu} = \sqrt{c_0^2 + \left(\frac{c_1}{E_{e,\mu}}\right)^2 + \left(\frac{c_2}{E_{e,\mu}}\right)^2} \tag{4.20}$$

$$\delta\theta^2_{e,\mu} = \sqrt{c_0^2 + \left(\frac{c_1}{E_{e,\mu}}\right)^2 + 2\left(\frac{c_2}{E_{e,\mu}}\right)^2} \tag{4.21}$$

$$\delta\theta^3_{e,\mu} = \sqrt{c_0^2 + \left(\frac{c_1}{E_{e,\mu}}\right)^2 + 3\left(\frac{c_2}{E_{e,\mu}}\right)^2} \tag{4.22}$$

$$\delta\theta^4_{e,\mu} = \sqrt{c_0^2 + \left(\frac{c_1}{E_{e,\mu}}\right)^2 + 4\left(\frac{c_2}{E_{e,\mu}}\right)^2} \tag{4.23}$$

We recall that we cannot distinguish the two particles in this angular region, therefore from now on we can refer to θ_{mu} and θ_e no more. Now we have just the measures of two angles given by each layer:

$$\begin{array}{lll} \text{layer 1:} & \hat{\theta}^1_a \pm \delta\theta^1_a, & \hat{\theta}^1_b \pm \delta\theta^1_b, \\ \text{layer 2:} & \hat{\theta}^2_a \pm \delta\theta^2_a, & \hat{\theta}^2_b \pm \delta\theta^2_b, \\ \text{layer 3:} & \hat{\theta}^3_a \pm \delta\theta^3_a, & \hat{\theta}^3_b \pm \delta\theta^3_b, \\ \text{layer 4:} & \hat{\theta}^4_a \pm \delta\theta^4_a, & \hat{\theta}^4_b \pm \delta\theta^4_b. \end{array} \tag{4.24}$$

We possess four measures for every detected particle. In order to have a single measure for the target outcoming angle, we make a reconstruction of the track. We use two methods of reconstruction: Kalman filter and least squares.

4.2.3 Tracking with Kalman filter

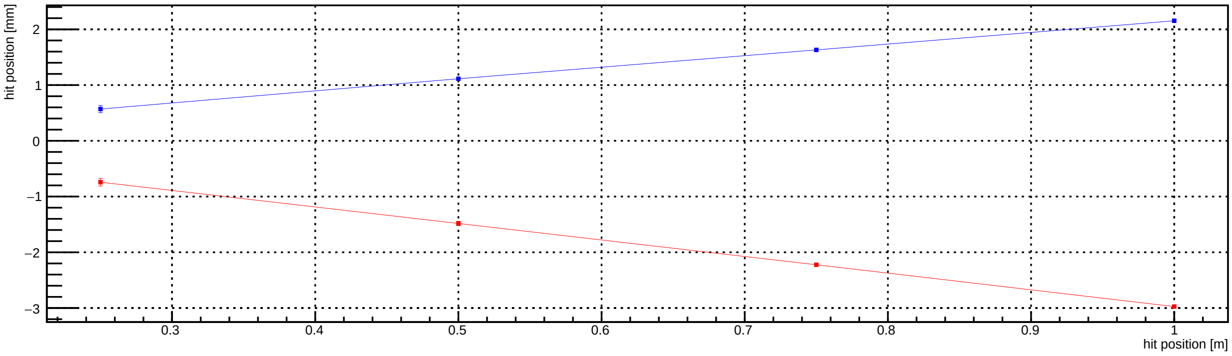

Figure 4.6: Example of hits distribution used for tracking.

The Kalman filter is a recursive process allowing to describe and to guess the evolution of the status of a dynamic system, subject to deterministic laws and noise, using repeated measurements. This algorithm is also implemented in the tracking processes to find the best trajectory for a given set of hits, even if not having a global information about the track. It is possible to show that the Kalman filter is equivalent to a tracking computation based on the least squares method.

The Kalman filter starts using the initial estimate for a quantity (in our case the outcoming track angle), the estimate for the uncertainty (the angular resolution), and the following measurement to predict the value of the observable at the best estimate. Going on with this process and adding new measurements the prediction becomes more and more accurate.

Consider a generic system whose status is described by the observable x, evolving in time from an observed state x_{k-1} to the subsequent x_k. The evolution equation can be written as:

$$\begin{aligned} x_k &= a x_{k-1} + w_k, \\ z_k &= x_k + v_k, \end{aligned} \tag{4.25}$$

where w_k is the noise in the system status evolution, z_k is the new experimental measurement with the corresponding uncertainty v_k.

The usage of the Kalman filter consists in two operations: (i) gain computation; (ii) present estimate computation. The Kalman gain determines the relative weight of the present estimate error p_{-1} and of the present experimental uncertainty r_k to determine the new prediction. It is defined as

$$g_k = \frac{p_{k-1}}{p_{k-1} + r_k}, \tag{4.26}$$

We can determine the present status as:

$$\begin{aligned} x_k &= x_{k-1} + g_k(z_k - x_{k-1}), \\ p_k &= (1 - g_k)p_{k-1}. \end{aligned} \tag{4.27}$$

Here x_k and p_k are the best estimates for the quantity x and for its error. They can be used in the next step of the iteration to predict a new value.

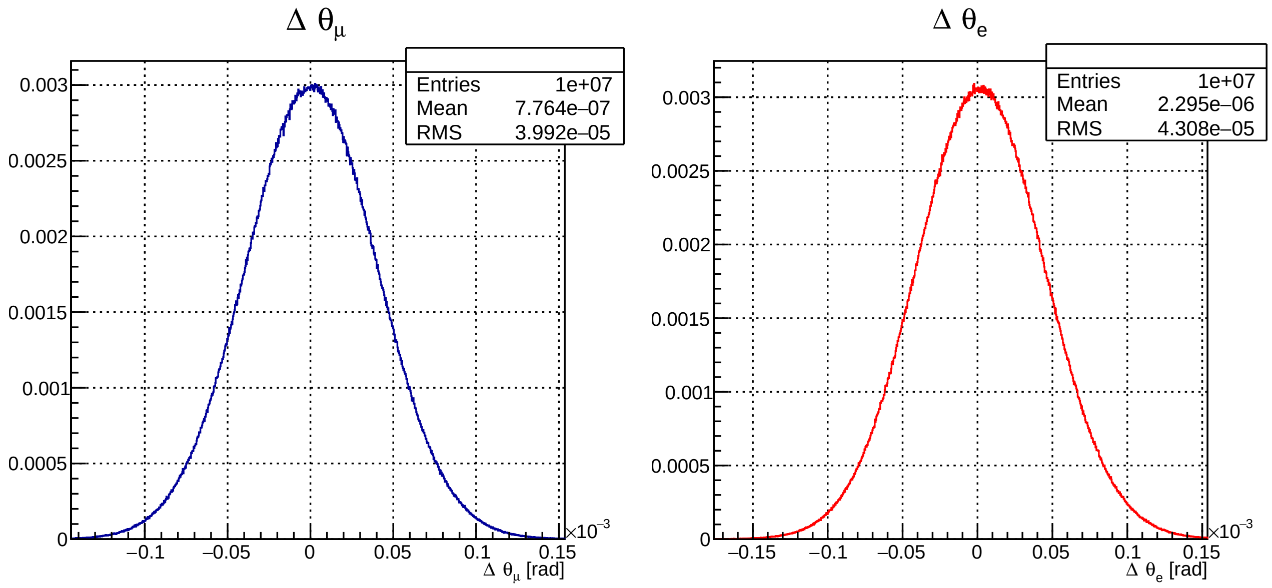

Figure 4.7: Difference between the outcoming particle angle and the reconstructed one $\Delta\theta_{e,\mu} = \theta_{e,\mu}^{true} - \theta_{e,\mu}^{Kalman}$, for the electron (right) and for the muon (left).

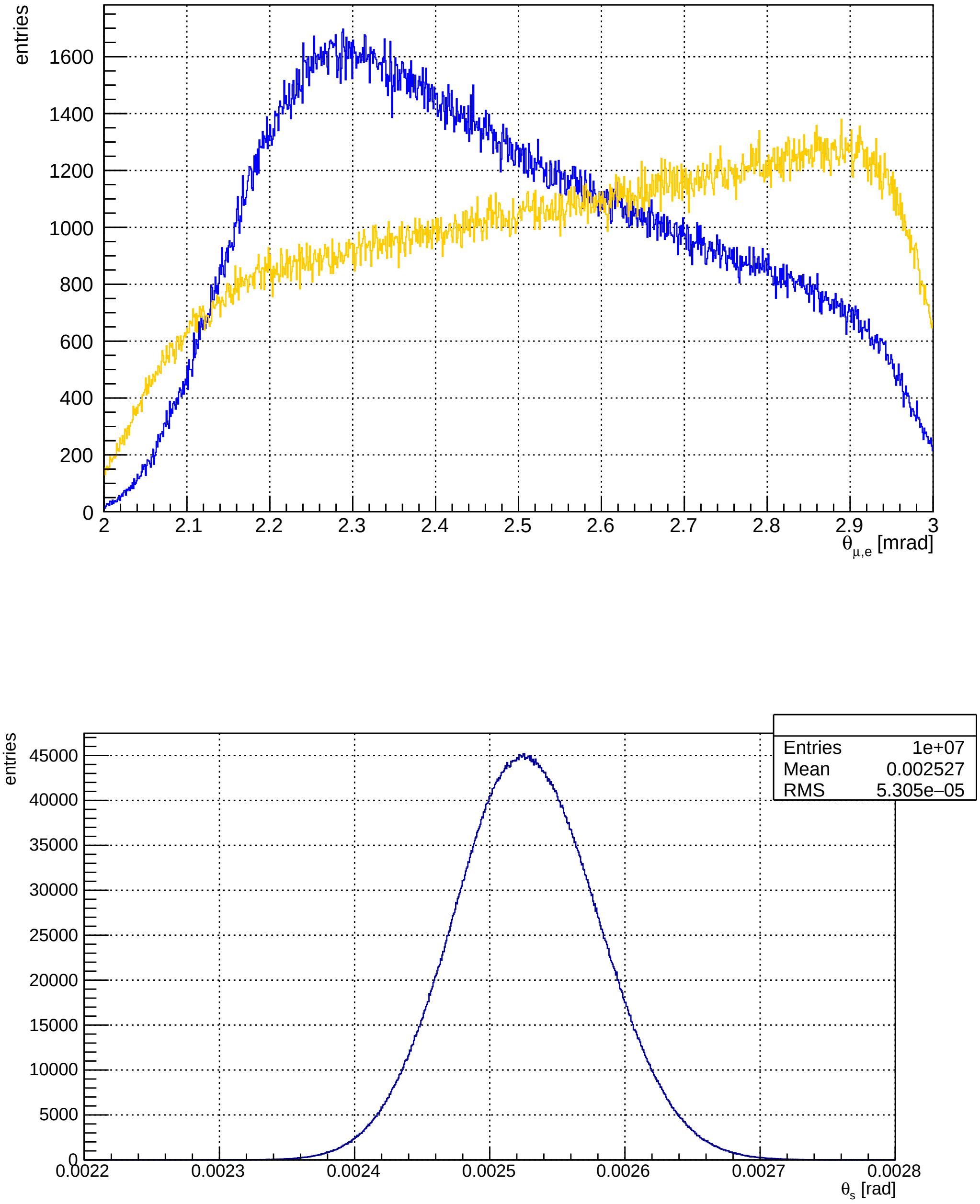

Figure 4.8: (top) Histogram showing the distribution of θ_μ in blue and θ_e in yellow. (bottom) Distribution of the angle θ_s used for the χ^2 test.

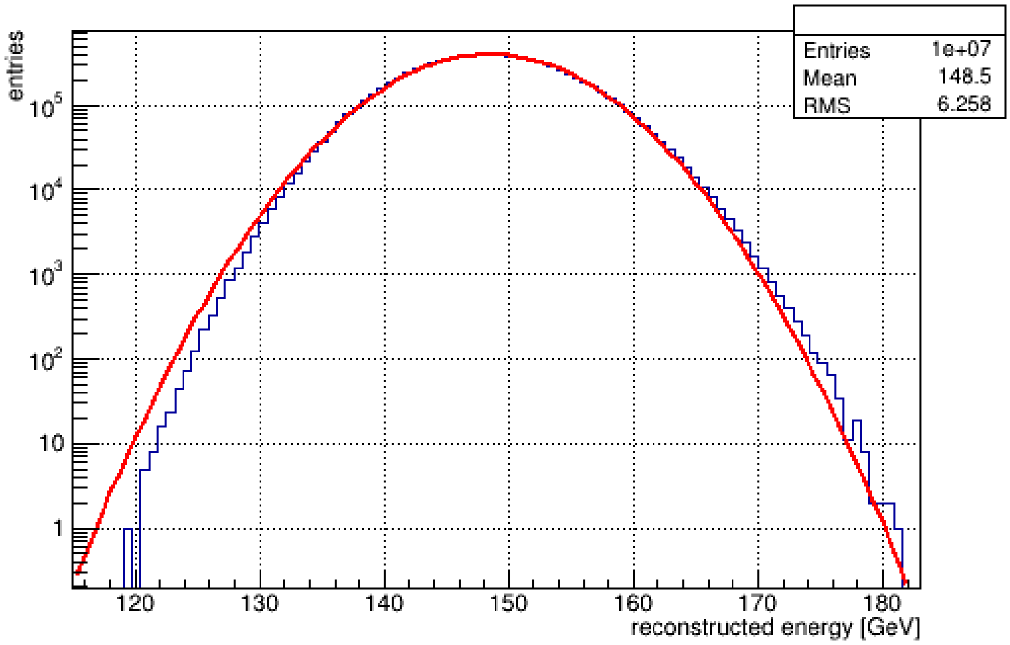

Figure 4.9: The reconstructed energy from the initial E_μ is no more gaussian. Note that the y-axis is shown in logarithmic scale.

4.3 Energy reconstruction with the template method

A naive approach to reconstruct the muon mean energy could be the following. We cound think to use the configuration where the two outcoming particle angles are similar. In this case one can use the Eq. (3.28)

$$\cos\theta_s \simeq \cos\theta_e = \frac{E_\mu + m_e}{\sqrt{E_\mu^2 - m_\mu^2}} \sqrt{\frac{E'_e - m_e}{E'_e + m_e}} \tag{4.28}$$

to determine E_μ.

The second term in the square root is with good approximation equal to 1 since $E'_e \gg m_e$. Recalling that $E_\mu = 150$ GeV and $\theta_e = \theta_\mu$ we have $E'_e = 75$ GeV, while $m_e = 0.510998$ MeV. Inverting this relation it gives

$$E_\mu^2(\cos^2\theta - 1) - E_\mu(2m_e) - m_e^2 - m_\mu^2\cos^2\theta = 0, \tag{4.29}$$

that can be solved for $E_\mu = E_\mu^{reco}$

$$E_\mu^{reco} = \frac{m_e - \sqrt{\cos^2\theta\big[(\cos^2\theta - 1)m_\mu^2 + m_e^2\big]}}{\cos^2\theta - 1}. \tag{4.30}$$

Filling a histogram with the value for E_μ^{reco} one gets the distribution shown in Fig. 4.9. It looks roughly similar to a gaussian (fit in red) but cannot be taken as a good solution for the muon mean energy due to the bias. This example shows that we cannot use the kinematic to reconstruct the muon mean energy with high precision, even neglecting the multiple scattering effect of the target and the intrinsic resolution of the tracking system. Therefore, we implemented another more refined method to get the muon mean energy E_μ, called "template method".

The procedure starts with the definition of the two outcoming angles (Fig. 4.8, top). We are interest in the region where $\theta_\mu \simeq \theta_e$ shown in Fig. 4.8. We generate a reference angular distribution for the θ_s angle, using a given value of the mean beam energy E_μ^{true}. The simulation is then repeated to generate new data sets using different muon mean energy values around E_μ^{true}. The distribution for θ_s obtained from the i-th generation can be compared to the reference one using a χ^2 test.

We expect that the plot of the χ^2 values as function of the muon mean energy corresponds to distribution with a minimum at the true energy value.

We determine $E_\mu^{ture} \simeq E_\mu^{best}$ searching for

$$\frac{\partial\chi^2(E_\mu)}{\partial E_\mu} = 0 \rightarrow \chi^2(E_\mu^{best}). \tag{4.31}$$

In order to get an uncertainty $\sim 1MeV$, in each simulation we must generate $\sim 10^7$ events. In fact the uncertainty on the mean angle related to the mean energy goes like:

$$\frac{\sigma}{\sqrt{N}} \simeq 1 \text{ MeV} , \tag{4.32}$$

where N is the size of the sample. Assuming $\sigma = 0.0375 \times 150.000 = 5.625$ GeV we must have

$$N = \frac{\sigma^2}{(10^{-3}\text{ GeV})^2} \simeq 10^7. \tag{4.33}$$

4.3.1 Implementing the χ^2 tests

Let us consider two histograms representing two different θ_s distributions: first simulation (having been obtained with a given energy $E_\mu^{true} \neq 150.000$ GeV) compared to the reference one (obtained with $E_\mu^{true} = 150.000$ GeV). These two histograms have the same number of bins r. We name the i-th bin content of two histograms respectively n_i and m_i. The total number of entries for the two histograms are

$$N = \sum_{i=1}^{r} n_i, \tag{4.34}$$

and

$$M = \sum_{i=1}^{r} m_i. \tag{4.35}$$

We assume that the two histograms represent two variables randomly distributed following approximately the same distribution. That's equivalent to assume the existence of r constants $p_1, ..., p_r$ such that

$$\sum_{i=1}^{r} p_i = 1, \tag{4.36}$$

and the probability for an entries to be in the i-th bin in both the histograms is p_i. The number of the entries in the i-th bin is a random value with a distribution that can be approximated to a Poisson distribution. For the first histogram we have

$$\frac{e^{-Np_i}(Np_i)^{n_i}}{n_i}, \tag{4.37}$$

for the second

$$\frac{e^{-Mp_i}(Mp_i)^{m_i}}{m_i}. \tag{4.38}$$

If the initial hypothesis is valid the maximum likelihood estimator for p_i with $i = 1, ..., r$ is

$$\hat{p}_i = \frac{n_i + m_i}{N + M}. \tag{4.39}$$

Therefore

$$\chi^2 = \sum_{i=1}^{r} \frac{(n_i - N\hat{p}_i)^2}{N\hat{p}_i} + \sum_{i=1}^{r} \frac{(m_i - M\hat{p}_i)^2}{M\hat{p}_i} = \frac{1}{MN} \sum_{i=1}^{r} \frac{(Mn_i - Nm_i)^2}{n_i + m_i} \tag{4.40}$$

is distributed as a $\chi^2_{(r-1)}$ distribution. Due to estimate the error associated with each χ^2 test, we use the usual error propagation for every bin n_i and m_i. In our case $M = N$, so the Eq. (E.1) becomes

$$\chi^2 = \sum_{i=1}^{r} \frac{(n_i - m_i)^2}{n_i + m_i}. \tag{4.41}$$

Each bin has a error that is

$$\delta n_i = \sqrt{n_i} \quad \text{e} \quad \delta m_i = \sqrt{m_i} \tag{4.42}$$

The error associated to the χ^2 test is found using the error propagation

$$\delta f(x, y) = \sqrt{\Big(\frac{\partial f}{\partial x}\delta x\Big)^2 + \Big(\frac{\partial f}{\partial y}\delta y\Big)^2}. \tag{4.43}$$

In our case

$$\frac{\partial f}{\partial x} = \frac{\partial \chi_i^2}{\partial n_i} = \frac{n_i - m_i}{(n_i + m_i)^2}\Big[n_i + 3m_i\Big], \tag{4.44}$$

$$\frac{\partial f}{\partial y} = \frac{\partial \chi_i^2}{\partial m_i} = \frac{n_i - m_i}{(n_i + m_i)^2}\Big[m_i + 3n_i\Big]. \tag{4.45}$$

the square sum of these two terms gives

$$\delta \chi_i^2 = \sqrt{\Big(\frac{\partial \chi^2}{\partial n_i}\delta n_i\Big)^2 + \Big(\frac{\partial \chi^2}{\partial m_i}\delta m_i\Big)^2}. \tag{4.46}$$

The square sum over each bin gives the final error for the χ^2 test obtained from the comparison of the two given simulations:

$$\delta \chi^2 = \sqrt{\sum_{i=1}^{r} \big(\delta \chi_i^2\big)^2}. \tag{4.47}$$

4.4 Results for simulations with 10^7 events

Once we have defined the angular distributions, we can find the minimum of the χ^2 curves:

$$\frac{\partial \chi^2}{\partial E_\mu} = 0 \rightarrow \chi^2_{min}. \tag{4.48}$$

The minimum of the χ^2 function corresponds to the best estimate we can achieve for the muon beam energy. We can estimate the error on the muon energy by finding the contour of E_μ corresponding to the χ^2 values between χ^2_{min} and $\chi^2_{min} + 1$.

In Figg. 4.10, 4.11 one can see the χ^2 obtained at different steps of the simulation (including different resolution effects). In Fig. 4.10-(top) we present the distribution obtained after the interaction. In Fig. 4.10-(bottom) it is shown instead the effect of the multiple scattering due to the target. To be noticed that the two distributions looks similar since the effect of the multiple scattering does not affect the angular distribution for this high energy values (75 GeV for both the outcoming muon and electron). In Fig. 4.11-(top) we present the χ^2 distribution after the complete reconstruction. In Fig. 4.11-(bottom) we show the χ^2 curves obtained fitting the thee distribution corresponding to three different conditions.

By applying the Kalman filter tracking method we get the following results

$$E_\mu^{best} = 150.001 \pm 0.003 \text{ GeV} \tag{4.49}$$

$$E_\mu^{best,Target} = 150.001 \pm 0.003 \text{ GeV}, \tag{4.50}$$

$$E_\mu^{best,Kalman} = 150.001 \pm 0.004 \text{ GeV}, \tag{4.51}$$

where E_μ^{best} is the muon mean energy value obtained with the template method considering only the spread of the muon beam energy (3.75%); $E_\mu^{best,Target}$ is the energy value obtained considering the effect of the multiple scattering in the target; $E_\mu^{best,Kalman}$ is the energy value obtained considering the entire tracking procedure.

The continuous curve superimposed to the χ^2 values represent the best fit of the data sets. They have been defined to determine the minimum and estimate the error.

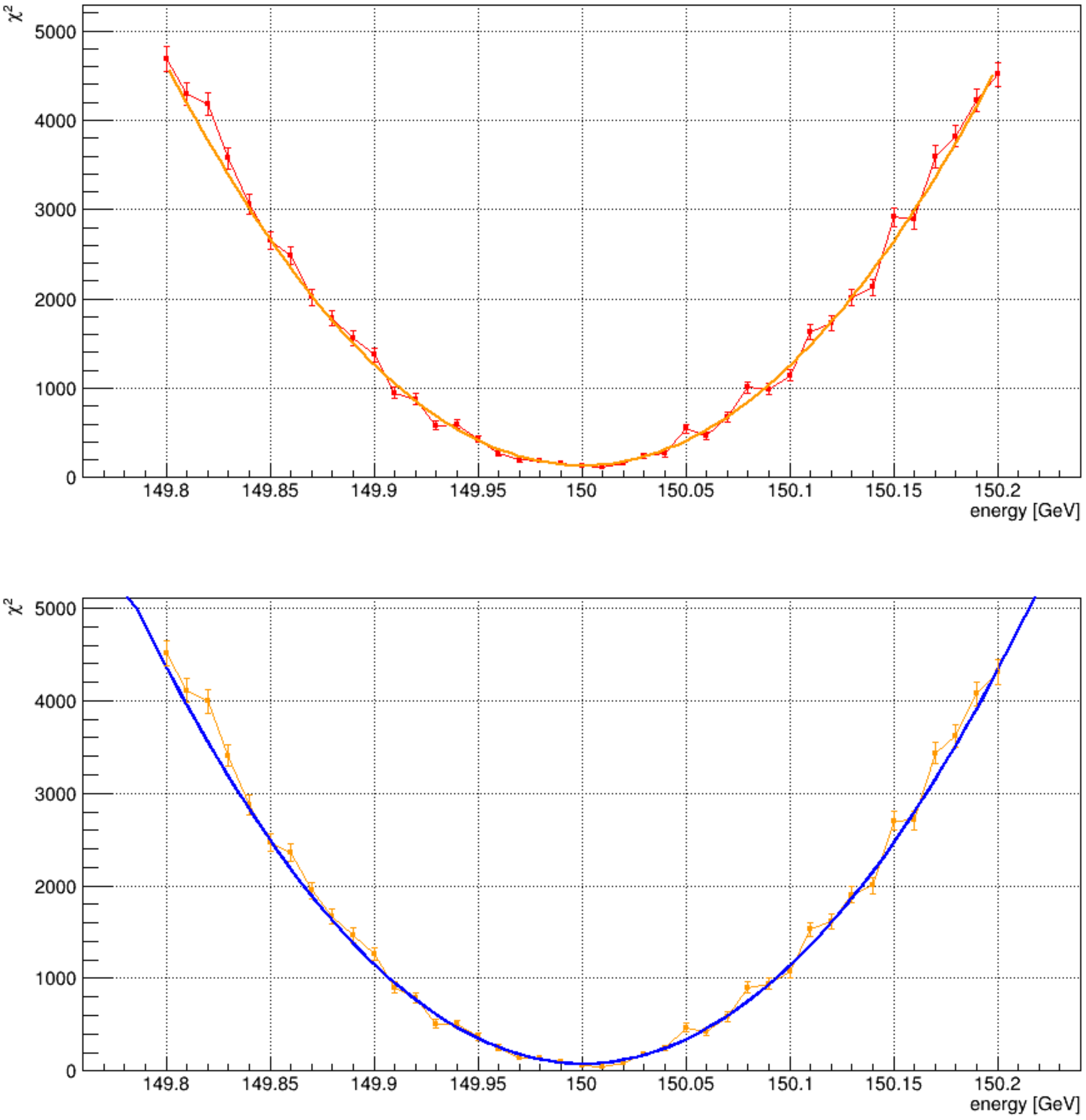

Figure 4.10: χ^2 values as a function of the muon mean energy used in the simulations. (top) We consider the value of θ_s been obtained considering only the spread of the muon beam energy (3.75%) and (bottom) adding the effect of the multiple scattering in the target.

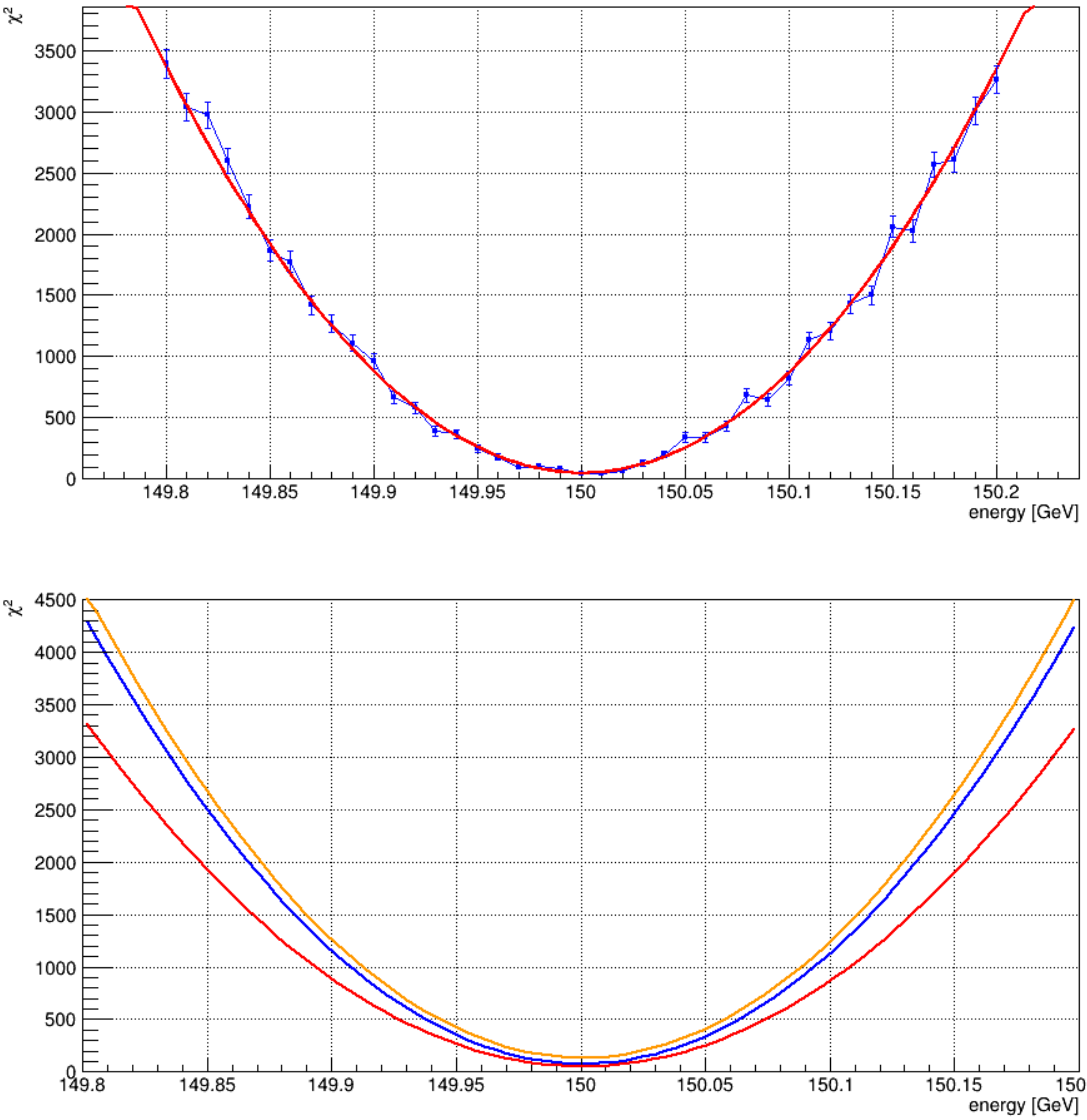

Figure 4.11: χ^2 values as a function of the muon mean energy used in the simulations. (top) We consider the value of θ_s obtained after the complete reconstruction using the Kalman filter method. (bottom) Comparison of the three χ^2 best fit functions obtained at the three different conditions.

We can observe that the estimated value of the muon mean energy E_μ^{best} due to the muon beam energy spread only is equal to the value one would get with an ideal tracking $E_\mu^{best,Target}$. This can be explained considering that in the equal angles condition, since the particle energies are rather high $E_\mu = E_e \simeq 75$ GeV, the multiple scattering does not affect the angular distribution (because of the $1/E$ dependence). The effect of the tracking performed, using the Kalman filter method, slightly worsten the precision varying from 3 to 4 MeV. The simulation shows that a remarkable precision of about 5 MeV on 150 GeV can be obtained allowing to determine the muon mean energy with the required precision.

Conclusions

We showed that the requirement of mesuring the muon beam mean energy with 5 MeV error can be achieved using a template method and the Kalman tracking procedure. In order to prove the feasibility e generated data samples simulating the MUonE detector response. The template method returns the χ^2 as a function of the muon beam mean energy. We showed that the minimum of the χ^2 distribution determines the mean very precisely.

We analyze the effect of the muon beam energy spread, of the multiple scattering due to the target thickness and the tracking precision, showing that the overall precision turns out to be within the required limit.

We did not study possible systematic effects as uncertainty on the multiple scattering model or the longitudinal detector positions. A more refined analysis of the systematic effects would be required and will be performed pursuing to possibly publish the results of this study.

Appendix A

Theoretical relativistic frame

In relativistic mechanics it is possible to define some Lorentz-invariant quantities, among these we recall the Mandelstam variables. For a scattering event as $p_\mu + p_e \rightarrow p'_\mu + p'_e$ they can be summarized as follows:

$$\begin{aligned} s &= (p_\mu + p_e)^2 = (p'_\mu + p'_e)^2 = \\ &= (E^*_\mu + E^*_e)^2 = (E^{*\prime}_\mu + E^{*\prime}_e)^2 = \\ &= m_\mu^2 + m_e^2 + 2m_e E_\mu; \end{aligned} \tag{A.1}$$

$$\begin{aligned} t &= (p_\mu - p'_\mu)^2 = (p_e - p'_e)^2 = \\ &= 2m_\mu^2 - 2E_\mu E'_\mu + 2P_\mu P'_\mu \cos\theta_\mu = \\ &= 2m_e^2 - 2m_e E'_e; \end{aligned} \tag{A.2}$$

$$\begin{aligned} u &= (p_\mu - p'_e)^2 = (p_e - p'_\mu)^2 = \\ &= m_\mu^2 + m_e^2 - 2E_\mu E'_e + 2P_\mu P'_e \cos\theta_e = \\ &= m_e^2 + m_\mu^2 - 2m_e E'_\mu. \end{aligned} \tag{A.3}$$

Only two in these variables are indipendent, and thus s, t, u can be related by the linear relation

$$\begin{aligned} s + t + u &= (p_\mu + p_e)^2 + (p - p)^2 + (p_e - p'_\mu)^2 = \\ &= p_\mu^2 + p_e^2 + p'^2_\mu + (p_\mu + p_e - p'_\mu)^2 = \\ &= 2m_e^2 + 2m_\mu^2. \end{aligned} \tag{A.4}$$

Now we can get the relation between s, t, u and other variables in the target system. From Eq.(A.1) we can write

$$E_\mu = \frac{s - m_\mu^2 - m_e^2}{2m_e}, \tag{A.5}$$

and consequently

$$\begin{aligned} P_\mu^2 &= E_e^2 - m_\mu^2 = \\ &= \left[(s - m_\mu^2 - m_e^2)^2 - 4m_\mu^2 m_e^2\right] \frac{1}{4m_e^2}. \end{aligned} \tag{A.6}$$

We write this result in the form

$$P_\mu = \frac{\lambda^{\frac{1}{2}}(s, m_\mu^2, m_e^2)}{2m_e} \tag{A.7}$$

by introducing the Kallen function

$$\begin{aligned} \lambda(x, y, z) &= (x - y - z)^2 - 4yz = \\ &= x^2 + y^2 + z^2 - 2xy - 2yz - 2zx. \end{aligned} \tag{A.8}$$

It is possible to write the initial-state quantities as

$$\begin{aligned} p_\mu &= \left(\frac{s - m_\mu^2 - m_e^2}{2m_e}, 0, 0, \frac{\lambda^{\frac{1}{2}}(s, m_\mu^2, m_e^2)}{2m_e}\right) \\ p_e &= (m_e, 0, 0, 0). \end{aligned} \tag{A.9}$$

We want to determine the energies (E_μ, E_e), the momenta (P_μ, P_e) and the angles (θ_μ, θ_e) in the final states. The energies are now most simply related to momentum transfers. For instance, from Eq. (A.2) we get directly

$$E_e' = \frac{2m_e^2 - t}{2m_e} \tag{A.10}$$

so that

$$P_e' = \frac{\lambda^{\frac{1}{2}}(t, m_\mu^2, m_e^2)}{2m_e}. \tag{A.11}$$

Similarly, from Eq. (A.3),

$$E_\mu' = \frac{m_e^2 + m_\mu^2 - u}{2m_e} \tag{A.12}$$

so that

$$P'_\mu = \frac{\lambda^{\frac{1}{2}}(u, m_e^2, m_\mu^2)}{2m_e}. \tag{A.13}$$

The angles θ_μ and θ_e are finally obtained from $t = (p_\mu - p'_\mu)^2$ and $u = (p_\mu - p'_e)^2$ with the result [11]

$$\cos\theta_\mu = \frac{(s - m_\mu^2 - m_e^2)(m_e^2 + m_\mu^2 - u) + 2m_e^2(t - 2m_\mu^2)}{\lambda^{\frac{1}{2}}(s, m_\mu^2, m_e^2)\lambda^{\frac{1}{2}}(u, m_e^2, m_\mu^2)} \tag{A.14}$$

and

$$\cos\theta_e = \frac{(s - m_\mu^2 - m_e^2)(2m_e^2 - t) + 2m_e^2(u - m_\mu^2 - m_e^2)}{\lambda^{\frac{1}{2}}(s, m_\mu^2, m_e^2)\lambda^{\frac{1}{2}}(t, m_e^2, m_e^2)} \tag{A.15}$$

Appendix B

Multiple scattering

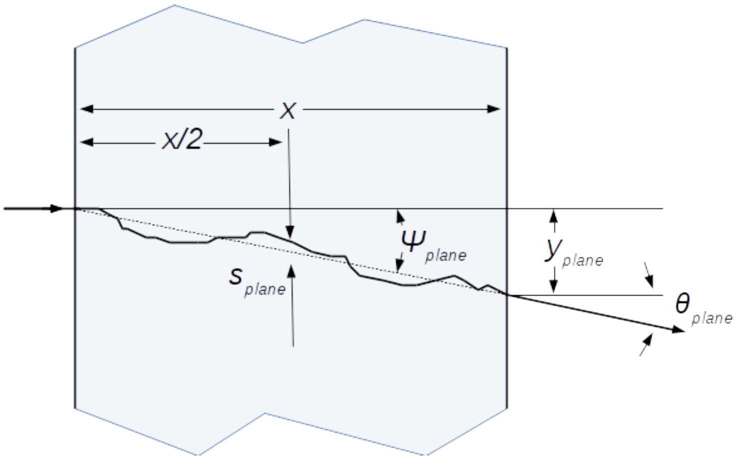

Figure B.1: Quantities used in the description of the multiple scattering process.

A charged particle traversing a medium is deflected by many small-angle elastic scattering events. Most of this deflection is due to Coulomb scattering from nuclei, hence the effect is called multiple Coulomb scattering. The Coulomb scattering distribution is well represented by the theory of Molière. It is roughtly Gaussian for small deflection angles, but at larger angles (greater than a few θ_0, defined below) it behaves like Rutherford scattering, with larger tails than does a Gaussian distribution.

If we define

$$\theta_0 = \theta^{rms}_{plane} = \frac{1}{\sqrt{2}}\theta^{rms}_{space} \tag{B.1}$$

then it is sufficient for many applications to use a Gaussian approximation with a width given by

$$\theta_0 = \frac{13.6MeV}{\beta cp} z\sqrt{\frac{x}{X_0}}\big[1 + 0.038\ln(\frac{x}{X_0})\big]. \tag{B.2}$$

Here p, βc and z are the momentum, velocity, and charge number of the incident particle, and x/X_0 is the thickness of the scattering medium in radiation lengths.

The nonprojected (space) and projected (plane) angular distributions are given approximately by

$$\frac{1}{2\pi\theta_0^2}\exp\left(-\frac{\theta_{space}^2}{2\theta_0^2}\right)d\Omega, \tag{B.3}$$

$$\frac{1}{\sqrt{2\pi}\theta_0}\exp\left(-\frac{\theta_{plane}^2}{2\theta_0^2}\right)d\theta_{plane}, \tag{B.4}$$

where θ is the deflection angle. In this approximation, $\theta_{space}^2 \approx (\theta_{plane,x}^2 + \theta_{plane,y}^2)$, where the x and the y axes are orthogonal to the direction of motion, and $d\Omega \approx \theta_{plane,x}\theta_{plane,y}$. Deflection into $\theta_{plane,x}$ and $\theta_{plane,y}$ are indipendent and identically distributed.

Appendix C

Muon energy loss

High-energy muons passing through matter loose energy due to electromagnetic processes. These are mainly ionization (order of α^2), bremmstrahlung (order of α^3), pair production (order of α^4) and photonuclear interactions.

The ionization loss of a muon of energy E is given by the Bethe-Bloch formula:

$$-\left\langle \frac{dE}{dx} \right\rangle = \alpha^2 4\pi N_a r_e^2 m_e \frac{Z}{A}\frac{1}{\beta^2}\left\{\frac{1}{2}\ln\frac{2m_e\beta^2\gamma^2 E_{max}}{I^2(Z)} - \beta^2 - \frac{\delta(\beta\gamma)}{2}\right\}, \tag{C.1}$$

where $\alpha = 1/137.036$ in the fine structure constant; $N = 6.023 \times 10^{23}$ is the Avogadro number; Z and A are the atomic number and the mass number of the medium; m_e and m_μ are the rest masses of the electron and the muon; $\beta = p/E$; $\gamma = E/m_\mu$; r_e is the compton wavelength of the electron; $I(Z)$ is the mean ionization potential of the medium; E_{max} is the maximum energy transferable to the electron,

$$E_{max} = 2m_e \frac{p^2}{m_e^2 + m_\mu^2 + 2m_e\sqrt{p^2 + m_\mu^2}}; \tag{C.2}$$

δ is the density correction.

As the particle energy increases, its electric field flattens and extends, so that the distant-collision contribution to Eq. (C.1) increases as $\ln\beta\gamma$. However, real media become polarized, limiting the field extension and effectively truncating this part of the logaritmic rise. At very high energies,

$$\delta/2 \to \ln(\hbar\omega_p/I) + \ln\beta\gamma - 1/2, \tag{C.3}$$

where $\delta(\beta\gamma)/2$ is the density effect correction introduced in Eq. (C.1) and $\hbar\omega_p$ is the plasma energy defined as

$$\hbar\omega_p = \sqrt{4\pi N_e r_e^3} m_e c^2/\alpha = \sqrt{\rho\langle Z/A\rangle} \times 28.816 eV \tag{C.4}$$

with N_e electron density (units of r_e^{-3}), ρ in g/cm^3. The density effect correction is usually computed as:

$$\delta(\beta\gamma) = \begin{cases} 2(ln10)x - \bar{C} & \text{if } x \geq x_1; \\ 2(ln10)x - \bar{C} + a(x_1 - x)^k & \text{if } x_0 \leq x \leq x_1; \\ 0 & \text{if } x < x_0(nonconductors); \\ \delta_0 10^{2(x-x_0)} & \text{if } x < x_0(conductors); \end{cases} \tag{C.5}$$

where $x = \log_{10}\eta = \log_{10}(p/Mc)$, M is the incident particle mass. $\bar{C}$ is obtained by equating the high-energy case of Eq. (C.5) with the limit given in Eq. (C.3), so that:

$$\bar{C} = 2\ln(I/\hbar\omega_p) + 1. \tag{C.6}$$

The other parameters $(a, k, x_0, x_1, \delta_0)$ are adjusted to give a best fit to the results of detailed numerical calculations for a logarithmically spaced grid of energy values.

The cross section for muon bremsstrahlung can be written as

$$\frac{d\sigma}{d\nu} = \alpha^3 \left(2Zr_3 \frac{m_e}{m_\mu}\right) \frac{1}{\nu} \left(\frac{4}{3} - \frac{4}{3}\nu + \nu^2\right) \phi(\delta), \tag{C.7}$$

where ν is the fraction of energy transferred to the photon. The following approximation for $\phi(\delta)$ are used

$$\phi(\delta) = \ln \frac{\frac{189 m_\mu}{m_e} Z^{-1/3}}{1 + \frac{189\sqrt{e}}{m_e}\delta Z^{-1/3}}, \text{ for } Z \leq 10 \tag{C.8}$$

$$\phi(\delta) = \ln \frac{\frac{2}{3}\frac{189 m_\mu}{m_e} Z^{-2/3}}{1 + \frac{189\sqrt{e}}{m_e}\delta Z^{-1/3}}, \text{ for } Z > 10 \tag{C.9}$$

where $\delta = m_\mu^2 \nu / 2E(1-\nu)$ is the minimum momentum tranfer to the nucleus and $e = 2.718$. The mean energy loss of

$$\frac{dE}{dx} = E\frac{N}{A}\int_{\nu_{min}}^{\nu_{max}} \nu \frac{d\sigma}{d\nu} d\nu \tag{C.10}$$

can be calculated analitically by solving the integral between $\nu_{min} = 0$ and $\nu_{max} = 1 - \frac{3}{4}\sqrt{e}(m_\mu/E)Z^{1/3}$. To account for bremmstrahlung losses on atomic electrons, Z^2 has been replaced with $Z(Z+1)$.

Anothe process that cause an energy loss for muon passing through a medium is the direct e^+e^- pair production in a Coulomb field. The average energy loss for pair production is calculated by numerical integration:

$$b_{pair,nucl} = -\frac{1}{E}\frac{dE}{dx}\bigg|_{pair,nucl} = \frac{N_a}{A}\int_0^1 \nu \frac{d\sigma}{d\nu} d\nu. \tag{C.11}$$

The same expression as for the nucleus is usually used to calculate the pair production contribution from atomic electrons, with Z^2 replaced with Z. A more precise method based on QED, gives a simpler formula which is valid to within 5% of the numerical result for $E > 5GeV$

$$b_{pair,elec} = -\frac{1}{E}\frac{dE}{dx}\bigg|_{pair,elec} = \frac{Z}{A}\left(0.073\ln\left(\frac{2E/M_\mu}{1+gZ^{2/3}E/M}\right) - 0.31\right) \times 10^{-6} cm^2/g. \tag{C.12}$$

Here $g = 4.4 \times 10^{-5}$ for hydrogen and $g = 1.95 \times 10^{-5}$ for other materials. [16]

Beryllium

Beryllium parameters necessary to calculate $-\langle dE/dx\rangle$ are: $Z = 4$; $A = 9.0121831 g/mol$; $\rho = 1.848 g/cm^3$; $I = 63.7 eV$; $a = 0.80392$; $k = m_s = 2.4339$; $x_0 = 0.0592$; $x_1 = 1.6922$; $\bar{C} = 2.7847$; $\delta_0 = 0.14$.

Muons through Beryllium

T MeV	p MeV/c	Ionization $MeV cm^2/g$	Bremsstrahlung $MeV cm^2/g$	Pair production $MeV cm^2/g$	Photonuclear effects $MeV cm^2/g$	Radiative losses $MeV cm^2/g$	dE/dx $MeV cm^2/g$
1.000×10^4	1.011×10^4	1.969	2.516×10^{-3}	2.479×10^{-3}	4.948×10^{-3}	9.943×10^{-3}	1.979
1.200×10^4	1.211×10^4	1.990	3.167×10^{-3}	3.271×10^{-3}	5.854×10^{-3}	1.229×10^{-2}	2.002
1.400×10^4	1.411×10^4	2.007	3.841×10^{-3}	4.109×10^{-3}	6.749×10^{-3}	1.470×10^{-2}	2.022
1.700×10^4	1.711×10^4	2.029	4.889×10^{-3}	5.437×10^{-3}	8.074×10^{-3}	1.840×10^{-2}	2.047
2.000×10^4	2.011×10^4	2.046	5.975×10^{-3}	6.839×10^{-3}	9.382×10^{-3}	2.220×10^{-2}	2.068
2.500×10^4	2.511×10^4	2.070	7.871×10^{-3}	9.352×10^{-3}	1.156×10^{-2}	2.879×10^{-2}	2.099
3.000×10^4	3.011×10^4	2.089	9.841×10^{-3}	1.201×10^{-2}	1.372×10^{-2}	3.557×10^{-2}	2.124
3.500×10^4	3.511×10^4	2.104	1.187×10^{-2}	1.479×10^{-2}	1.585×10^{-2}	4.251×10^{-2}	2.147
4.000×10^4	4.011×10^4	2.118	1.396×10^{-2}	1.767×10^{-2}	1.796×10^{-2}	4.959×10^{-2}	2.167
4.500×10^4	4.511×10^4	2.129	1.609×10^{-2}	2.065×10^{-2}	2.005×10^{-2}	5.679×10^{-2}	2.186
5.000×10^4	5.011×10^4	2.140	1.826×10^{-2}	2.371×10^{-2}	2.213×10^{-2}	6.410×10^{-2}	2.204
5.500×10^4	5.511×10^4	2.149	2.047×10^{-2}	2.682×10^{-2}	2.425×10^{-2}	7.154×10^{-2}	2.221
6.000×10^4	6.011×10^4	2.157	2.271×10^{-2}	3.001×10^{-2}	2.636×10^{-2}	7.908×10^{-2}	2.236
7.000×10^4	7.011×10^4	2.172	2.730×10^{-2}	3.655×10^{-2}	3.056×10^{-2}	9.441×10^{-2}	2.267
8.000×10^4	8.011×10^4	2.185	3.199×10^{-2}	4.330×10^{-2}	3.473×10^{-2}	1.100×10^{-1}	2.295
9.000×10^4	9.011×10^4	2.196	3.677×10^{-2}	5.023×10^{-2}	3.888×10^{-2}	1.259×10^{-1}	2.322
1.000×10^5	1.001×10^5	2.206	4.163×10^{-2}	5.731×10^{-2}	4.301×10^{-2}	1.420×10^{-1}	2.348
1.200×10^5	1.201×10^5	2.223	5.149×10^{-2}	7.147×10^{-2}	5.142×10^{-2}	1.744×10^{-1}	2.397
1.400×10^5	1.401×10^5	2.237	6.158×10^{-2}	8.603×10^{-2}	5.979×10^{-2}	2.074×10^{-1}	2.444
1.700×10^5	1.701×10^5	2.254	7.758×10^{-2}	1.058×10^{-1}	7.231×10^{-2}	2.579×10^{-1}	2.512

Table C.1: dE/dx values for muons passing through Beryllium with energies between $3.182 \times 10^2 MeV$ (minimum ionization) and $170 GeV$. Different physical processes are separated. [ref. PDG]

Appendix D

Tracking with least squares

The multiple scattering effect produces errors correlated from one layer to the next. A scattering event in layer 1 produces correlated errors in layer 2, 3 and 4. The proper error matrix is not diagonal, and must find out.

We denote δx_i the track deviation x-coordinate point on the i-th layer, with respect to the initial incident direction. [15]

$$\begin{aligned}
\delta x_1 &= 0; \\
\delta x_2 &= \delta_1; \\
\delta x_3 &= \delta_{31} + \delta_2; \\
\delta x_4 &= \delta_{41} + \delta_{42} + \delta_3;
\end{aligned} \tag{D.1}$$

where the individual contributions due to proceding ascatterings are

$$\begin{aligned}
\delta_{31} &= \delta_1 \frac{z_3 - z_1}{z_2 - z_1}; \\
\delta_{41} &= \delta_1 \frac{z_4 - z_1}{z_2 - z_1}; \quad \delta_{42} = \delta_2 \frac{z_4 - z_2}{z_3 - z_2}.
\end{aligned} \tag{D.2}$$

The the errors due to the multiple scattering are statistical variables, therefore it is necessary to find their mean value, and express it by indipendent scattering deviations δ_k, unaffected by earlier scatterings

$$\delta_k \equiv \sqrt{\langle \delta_k^2 \rangle} = \theta^M_{\mu,e}\big(z_{k+1} - z_k\big). \tag{D.3}$$

We express the δx_i deviations by the indipendent δ_k ones (D.3), for which $\langle \delta_k \rangle = 0$

$$\delta x_i = \sum_{k=1}^{i-1} \delta_k \frac{z_i - z_k}{z_{k+1} - z_k}. \tag{D.4}$$

The position error covariance matrix (V_{ij}) is defined as the statistical mean of the pair deviation products $\langle \delta x_i \delta x_j \rangle$ for all possible detection layers. It is

$$\begin{aligned} &V_{ij} \equiv \langle \delta x_i \delta x_j \rangle = \\ &(\theta^M_{\mu,e})^2 \big[(z_i - z_1)(z_j - z_1) + (z_i - z_2)(z_j - z_2) + ... + (z_i - z_{i-1})(z_j - z_{i-1})\big] \\ &\text{for } i \leq j = 1, 2, ..., n. \end{aligned} \tag{D.5}$$

The (V_{ij}) matrix is symmetric.

In our case, considering a muon and an electron both with an energy of $\sim 75 GeV$, the simulated system configuration ($z_1 = 0.25$ m, $z_1 = 0.5$ m, $z_1 = 0.75$ m, $z_1 = 1$ m), with an intrinsic resolution of $\sim 2\mu$m, the matrix elements V_{ij} (in squared centimeters) is:

$$V = \begin{pmatrix} 1 & 0 & 0 & 0 \\ 0 & 2.04658 \times 10^{-11} & 4.09316 \times 10^{-11} & 6.1397 \times 10^{-11} \\ 0 & 4.09316 \times 10^{-11} & 1.02329 \times 10^{-10} & 1.63726 \times 10^{-10} \\ 0 & 6.1397 \times 10^{-11} & 1.63726 \times 10^{-10} & 2.86521 \times 10^{-10} \end{pmatrix}. \tag{D.6}$$

Now we can use this matrix to recontruct the track by a least squares fit procedure. We are interested in the relation

$$x = x_0 + \alpha_x z \tag{D.7}$$

which describes a straight particle track in two dimensions. It is possible to express the χ^2 in matrix form as

$$\chi^2 = \big(X - HA\big)^T V^{-1} \big(X - HA\big) \tag{D.8}$$

where

$$X = \begin{pmatrix} x_1 \\ x_2 \\ x_3 \\ x_4 \end{pmatrix}; \quad H = \begin{pmatrix} 1 & z_1 \\ 1 & z_2 \\ 1 & z_3 \\ 1 & z_4 \end{pmatrix}; \quad A = \begin{pmatrix} x_0 \\ \alpha_x \end{pmatrix}. \tag{D.9}$$

As required by the least squares procedure, we impose

$$\frac{\partial \chi^2}{\partial A} = 0, \text{ that is } H^T V^{-1}(X - HA) = 0. \tag{D.10}$$

By solving the linear system relative to A we get the fit parameters

$$A = (H^T V^{-1} H)^{-1} (H^T V^{-1} X). \tag{D.11}$$

Appendix E

Pearson's χ^2 test

We try to examine a goodness-of-fit test that can be applied to the distribution of a variable x. We start considering a histogram of the observed x values with N bins. Suppose the number of entries in bin i is n_i, and the number of expected entries is ν_i. We construct a method to evalutate the level of agreement between the observed and the expected histograms. The most commonly used goodness-of-fit test is based on Pearson's χ^2 statistic,

$$\chi^2 = \sum_{i=1}^{N} \frac{(n_i - \nu_i)^2}{\nu_i}. \tag{E.1}$$

If the data $n = (n_1, ..., n_N)$ are Poisson distributed with mean values $\nu = (\nu_1, ..., \nu_N)$, and if the number of entries in each bin is not too small ($n_i \geq 5$) then one can show that the statistic (E.1) will follow a χ^2 distribution,

$$f(z, n) = \frac{1}{2^{n/2}\Gamma(n/2)} z^{n/2-1} e^{-z/2}, n = 1, 2, ..., \tag{E.2}$$

for N degrees of freedom. This hold regardless of the distribution of the variable x; the χ^2 test is therefore said to be distribution free. The restriction on the number of entries is equivalent to the requirement that the n_i be approximately Gaussian distributed.

Since the standard deviation of a Poisson valiable with mean ν_i is equal to $\sqrt{\nu_i}$ the χ^2 statistic gives the sum of squares of the deviations between observed and expected values, measured in units of the corresponding standard deviations. A larger χ^2 thus corresponds to a larger discrepancy between data and the hypotesis. The P-value or significance level is therefore given by the integral of the χ^2 distribution from the observed χ^2 to infinity,

$$P = \int_{\chi^2}^{\infty} f(z, n_d) dz, \tag{E.3}$$

where here the number of degrees of freedom is $n_d = N$. The ratio χ^2/n_d is therefore quoted as a measure of agreement between data and hypothesis.

The correct P-value con be obtained by determing the distribution of the statistic with a Monte Carlo program. This is done by generating Poisson values n_i for each bin based on the mean values ν_i, and then computing and recording the χ^2 value. [17]

Bibliography

[1] G.W. Bennett *et al.*, Phys. Rev. Lett. **89**, 101804 (2002);
Erratum *ibid.*Phys. Rev. Lett. **89**, 129903 (2002);
G.W. Bennett *et al.*, Phys. Rev. Lett. **92**, 161802 (2004);
G.W. Bennett *et al.*, Phys. Rev. **D73**, 072003 (2006).

[2] J. J. Sakurai, *Modern Quantum Mechanics*, Pearson, 2nd ed., 2010.

[3] M. Tanabashi et al., *Particle Data Group*, Phys. Rev. D **98**, 030001 (2018).

[4] F. Jegerlehner, *The anomalous magnetic moment of the muon*, Springer Tracts Mod. Phys. **226**, 2008.

[5] M. Davier *et al.*, Eur. Phys. J. **C71**, 1515 (2011).

[6] R. Alemany *et al.*, Eur. Phys. J. **C2**, 123 (1998).

[7] F. Jegerlehner and A. Nyffeler, Phys. Reports **477**, 1 (2009).

[8] K. Hagiwara *et al.*, J. Phys. **G38**, 085003 (2011).

[9] M. Davier *et al.*, arXiv:1706.09436 (2017).

[10] J. Prades, E. de Rafael, A. Vainshtein, *Hadronic Light-by-Light Scattering Contribution to the Muon Anomalous Magnetic Moment*, arXiv:0901.0306 (2009).

[11] E. Byckling, K. Kajantie *Particle Kinematics*, John Wiley & Sons, 1973.

[12] G. Abbiendi *et al.*, *Measuring the leading hadronic contribution to the muon g-2 via μe scattering*, Eur. Phys. J. C **77** (2017).

[13] G. Abbiendi *et al*, *Measuring the leading hadronic contribution to the muon g-2 via μe scattering*, Eur. Phys. J. C (2017) 77: 139.

[14] The MUonE Collaboration, *Letter of Intent: The MUonE Project*, CERN-SPSC-2019-026.

[15] M. Pentia, G. Iorgovan, A. Mihul, *Multiple scattering error propagation in particle track reconstruction*, arXiv:hep-ex/9406006v1 (1994).

[16] W. R. Leo, *Techniques for Nuclear and Particle Physics Experiments*, Springer, 1987.

[17] G. Cowan, *Statistical Data Analysis*, Oxford University Press, 1998.